12-2022

Comparison of a Dynamic Ankle Orthosis to a Walking Boot for Preserving Ankle Joint Motion and Reducing Tibial Bone Load and Strain

Perri Johnson Jr.

Comparison of a Dynamic Ankle Orthosis to a Walking Boot for Preserving Ankle Joint Motion and Reducing Tibial Bone Load and Strain

Abstract

Tibial stress fractures are a common overuse injury accounting for 21.9 – 69% of stress fractures among runners and 24 – 51.2% of stress fractures in military cadets. Current treatment involves wearing a walking boot for 3 – 12 weeks, which limits ankle motion and causes lower limb muscle atrophy. A Dynamic Ankle Orthosis (DAO) provided a distractive force that offloaded the ankle and retained sagittal ankle excursion during walking. It remains unclear how tibial loading is affected by a walking boot or the DAO. This thesis presents a feasibility study confirming the offloading effects of the DAO on tibial loads and Achilles tendon forces during treadmill walking, and a cadaveric study evaluating the offloading effects of the DAO on distal tibia strain. The objective of study 1 was to determine the effects of the DAO and walking boot on tibial compressive force and ankle motion during treadmill walking. Twenty healthy young adults walked on a split-belt instrumented treadmill at 1.0 m/s in two brace conditions: DAO and walking boot. A 3D motion capture system recorded kinematic data, force treadmill recorded ground reaction forces, and vertical force insoles measured in-shoe vertical reaction force. Kinetic and kinematic variable calculations were used to determine the peak tibial compressive force. Target offloading of the DAO was 10% body weight. The DAO moderately reduced peak tibial compressive force (10.9%) and Achilles tendon force (12%) compared to the walking boot. Sagittal plane ankle motion during stance phase was largely reduced by 54.9% in the walking boot compared to the DAO. The objective of study 2 was to evaluate changes in strain magnitude due to the offloading effect of the DAO on tibial bone mechanics compared to standard-of-care walking boot using fresh frozen cadaver specimens. Three fresh frozen cadaver legs were placed in a robotic testing platform and dynamically loaded to 900N at a rate of 3.2mm/s in the DAO and walking boot. Linear strain gauges were attached to the distal tibia and midshaft tibia to measure the compressive strain at specific points along the longitudinal axis of the tibia. Vertical force sensing insoles measured in-shoe vertical reaction force. Target offloading of the DAO was 10% of the applied load. Peak strain was significantly reduced at the distal tibia (23.31%) wearing the DAO compared to the walking boot. Pearson correlations showed moderate to strong negative linear relationship between the compressive strain and vertical reaction force measurements within subjects at both the distal and midshaft tibia. These findings indicate the DAO moderately reduced tibial compression force and Achilles tendon force while providing greater sagittal ankle excursion compared to a walking boot. In addition to reproducing similar strain data to previous literature, the DAO strongly reduced the peak strain primarily at the distal tibia as well as reduced vertical reaction force. Moderate to strong linear correlations occurred between the external vertical reaction force and internal strain magnitude. This body of work provides evidence that the DAO could function as an alternative rehabilitation device for treating tibial stress fractures by reducing bone strain and tibial loading during walking.

Document Type

Thesis

Degree Name

Master of Science (MS)

Program

Biomedical Engineering

Research Advisor

Denis J. DiAngelo, PhD

Keywords

Offload, Tibial Bone Strain, Tibial Compressive Force, Tibial Stress Fractures, Walking Boot

Subject Categories

Analytical, Diagnostic and Therapeutic Techniques and Equipment | Investigative Techniques | Medicine and Health Sciences | Orthopedics | Orthotics and Prosthetics | Other Medicine and Health Sciences | Rehabilitation and Therapy | Sports Sciences

UNIVERSITY OF TENNESSEE HEALTH SCIENCE CENTER

MASTER OF SCIENCE THESIS

Comparison of a Dynamic Ankle Orthosis to a Walking Boot for Preserving Ankle Joint Motion and Reducing Tibial Bone Load and Strain

Author:
Perri Johnson, Jr.

Advisor:
Denis J. DiAngelo, PhD

A Thesis Presented for The Graduate Studies Council of
The University of Tennessee Health Science Center
in Partial Fulfillment of the Requirements for the Master of Science degree
In the Joint Graduate Program in Biomedical Engineering
From the University of Tennessee and University of Memphis

in

Biomedical Engineering: Biomechanics
College of Graduate Health Sciences

December 2022

DEDICATION

First, I want to thank God for blessing and providing me with an amazing opportunity and knowledge to continue my education at The University of Tennessee Health Science Center. To my parents, Perri A. Johnson Sr. and Stephanie R. Johnson, my little brother, Taylor J. Johnson, and all my close friends and family, for their constant love and support throughout my studies.

ACKNOWLEDGEMENTS

I am thankful to God for blessing me with a great opportunity to further fulfill my purpose in life for His glory. I would like to thank my advisor, Dr. Denis J. DiAngelo, who has repeatedly pushed me outside of my comfort zone throughout the course of my studies to help me grow as a researcher. I would like to thank my committee members, Dr. Max Paquette and Dr. Richard Kasser for their guidance and support during my time at the University of Tennessee Health Science Center. I would like to thank the College of Graduate Health Sciences for granting me Travel Awards for financial assistance for me to attend the North American Congress on Biomechanics conference and Biomedical Engineering Society Meeting. Thank you to the research grant from the University of Tennessee Research Foundation to develop the technology in United States Patent Application 20210259871, Published Date: Aug. 26, 2021: DiAngelo D, Chung C, Parker M., "DYNAMIC ANKLE ORTHOSIS DEVICES, SYTEMS, AND METHODS."

I would like to thank each person who aided during the testing of the Dynamic Ankle Orthosis (DAO): I cannot thank you enough for volunteering your time and feedback. I would like to acknowledge my fellow students in the UTHSC Orthopedic Biorobotics and Rehabilitation Laboratory, Kirsten Miller, Lyndsey Bouve, Alexis Nelson Chase Mareno, and Lisa Phan for their support and contributions at each phase of this research.

Finally, I would like to thank the students in the University of Memphis Musculoskeletal Analysis Lab, Adriana Miltko, Zoey Kearns, Hailey Fong, William Crosslin, Julie Storey, Garrett Hess, and Eduardo Martinez for their assistance in learning testing equipment, data processing, and experimental testing of the DAO. Finally, I would like to thank my family and friends for providing me with constant support and encouragement throughout every aspect of my life, and without whom I would not have the courage to continue pursuing the path God has intended for me.

ABSTRACT

Tibial stress fractures are a common overuse injury accounting for 21.9 – 69% of stress fractures among runners and 24 – 51.2% of stress fractures in military cadets. Current treatment involves wearing a walking boot for 3 – 12 weeks, which limits ankle motion and causes lower limb muscle atrophy. A Dynamic Ankle Orthosis (DAO) provided a distractive force that offloaded the ankle and retained sagittal ankle excursion during walking. It remains unclear how tibial loading is affected by a walking boot or the DAO. This thesis presents a feasibility study confirming the offloading effects of the DAO on tibial loads and Achilles tendon forces during treadmill walking, and a cadaveric study evaluating the offloading effects of the DAO on distal tibia strain.

The objective of study 1 was to determine the effects of the DAO and walking boot on tibial compressive force and ankle motion during treadmill walking. Twenty healthy young adults walked on a split-belt instrumented treadmill at 1.0 m/s in two brace conditions: DAO and walking boot. A 3D motion capture system recorded kinematic data, force treadmill recorded ground reaction forces, and vertical force insoles measured in-shoe vertical reaction force. Kinetic and kinematic variable calculations were used to determine the peak tibial compressive force. Target offloading of the DAO was 10% body weight. The DAO moderately reduced peak tibial compressive force (10.9%) and Achilles tendon force (12%) compared to the walking boot. Sagittal plane ankle motion during stance phase was largely reduced by 54.9% in the walking boot compared to the DAO.

The objective of study 2 was to evaluate changes in strain magnitude due to the offloading effect of the DAO on tibial bone mechanics compared to standard-of-care walking boot using fresh frozen cadaver specimens. Three fresh frozen cadaver legs were placed in a robotic testing platform and dynamically loaded to 900N at a rate of 3.2mm/s in the DAO and walking boot. Linear strain gauges were attached to the distal tibia and midshaft tibia to measure the compressive strain at specific points along the longitudinal axis of the tibia. Vertical force sensing insoles measured in-shoe vertical reaction force. Target offloading of the DAO was 10% of the applied load. Peak strain was significantly reduced at the distal tibia (23.31%) wearing the DAO compared to the walking boot. Pearson correlations showed moderate to strong negative linear relationship between the compressive strain and vertical reaction force measurements within subjects at both the distal and midshaft tibia.

These findings indicate the DAO moderately reduced tibial compression force and Achilles tendon force while providing greater sagittal ankle excursion compared to a walking boot. In addition to reproducing similar strain data to previous literature, the DAO strongly reduced the peak strain primarily at the distal tibia as well as reduced vertical reaction force. Moderate to strong linear correlations occurred between the external vertical reaction force and internal strain magnitude. This body of work provides evidence that the DAO could function as an alternative rehabilitation device for treating tibial stress fractures by reducing bone strain and tibial loading during walking.

TABLE OF CONTENTS

LIST OF TABLES

LIST OF FIGURES

LIST OF ABBREVIATIONS

AFO	Ankle Foot Orthosis
a_y	Linear Acceleration
a_z	Vertical Acceleration
BW	Body Weight
CON	Control
DAO	Dynamic Ankle Orthosis
DUAFO	Double Upright Ankle Foot Orthosis
F_{AT}	Achilles Tendon Force
F_A	Force acting along the longitudinal axis of the tibia
F_{tibia}	Peak Tibial Compressive Force
F_z'	Summation of forces at the ankle joint
GRF	Ground Reaction Force
GRF_y	Propulsive Ground Reaction Force
I_A	Ankle Moment of Inertia
M_A	Ankle Moment
M_F	Mass of the Foot
ROM	Range of Motion
TSF	Tibial Stress Fracture
VRF	Vertical Reaction Force
VRFz	Insole Vertical Reaction Force
y_{A1}	Vertical Acceleration Moment Arm
y_{A2}	Insole Vertical Reaction Force Moment Arm
z_{A1}	Linear Acceleration Moment Arm
z_{A1+A2}	Propulsive Ground Reaction Force Moment Arm
3D	Three Dimensional

CHAPTER 1. INTRODUCTION

Approximately 70% of all sports related bone stress fractures are running related [1]. Tibial stress fractures (TSF) are one of the most common overuse injuries due to repeated submaximal loading, causing the mechanical properties of bone to fatigue over time [2,3] accounting for 69% of TSF injuries in recreational runners [1] and 29% of TSF injuries in military personnel [4]. Several military studies have found that women are twice as likely to experience a stress fracture due to factors such as reduced tibial cross-sectional area and bone mineral density compared to men, as well as increased foot pronation [5-7].

Conservative treatment options aim to reduce pain during weight bearing activities, progressively re-introduce loads at the injured site to prevent re-injury and prevent prolonged healing [8, 9]. Prescription of a clinical walking boot serves to immobilize the ankle joint and stabilize the lower limb and foot to aid in healing. Previous research has shown reduced plantar pressure under the foot [10,11]. However, increases in heel pressure have been reported [12], providing contradicting findings if the loads on the tibia are reduced by a walking boot. The majority of studies that examine TSFs in a walking boot are clinical studies that do not analyze the loading mechanics of the tibia during weight bearing events [4,13,14]. Additionally, immobilization of the lower leg results in a significant reduction of ankle mobility. Leading to muscle atrophy of the plantarflexor muscles, prolonging an athlete's recovery and return to sport.

The Dynamic Ankle Orthosis (DAO) was originally designed to manage mechanical pain and restore function to individuals suffering from orthopedic foot and ankle conditions [15]. The device uses pneumatic cylinders to apply a distractive force across the ankle joint and lower extremity that reduces the mechanical forces acting on the tibia while allowing unconstrained ankle rotation during level walking [15,16]. This study investigates the feasibility of using the DAO as a method for treating tibial stress fractures by reducing loads across the fracture site thereby reducing muscle atrophy and enabling bone remodeling sooner in the recovery phase.

The organization of this thesis is as follows: Chapter 2 presents background information and literature review to provide motivation for this work. Chapter 3 details a functional treadmill walking analysis of tibial compressive force with twenty healthy individuals comparing the DAO to a standard of care walking boot. Chapter 4 details a cadaveric study performed with three fresh frozen cadavers to analyze how strain measurements are affected at common tibial stress fracture sites while wearing the DAO or walking boot. Chapter 5 provides discussion relating the findings between the treadmill walking assessment presented in Chapter 3 and the cadaveric assessment presented in Chapter 4. Chapter 6 provides an overview of future work to assess EMG muscle activity of the lower leg between the DAO and a walking boot during walking, and an overview of a clinical study outfitting tibial stress fracture patients with the DAO or walking boot and monitoring the rate of bone union and muscle atrophy, and lastly, a

possible *in vivo* study involving direct measures of tibial bone strain under various loading conditions and activities.

CHAPTER 2. BACKGROUND

This chapter is intended to provide a foundational understanding for the material that is covered within the content of this thesis. Specifically, this chapter offers relevant terminology and a literature review to provide the reader with foundational information for the proceeding work.

Anatomy of the Lower Leg

To understand the basic concepts of biomechanics described within this thesis an understanding of the anatomical vocabulary within the field of biomechanics is crucial. The human body is divided into three anatomical planes of movement as shown in **Figure 2-1**. The frontal/coronal plane (divides the body into front and back regions), the midsagittal plane (divides the body into left and right regions), and the transverse/horizontal plane (divides the body, at the waist, into the top and bottom regions). Anatomical relationships are used to describe the relative position in relation to various body parts. Superior (toward the head), inferior (toward the feet), anterior (toward the front of the body), posterior (toward the back of the body), medial (closer to the median of the body or midline of a segment), lateral (further from the median plane of the body or midline of a segment), proximal (closer to the trunk), Distal (farther from the trunk), superficial (closer to the surface), deep (farther from the surface). Ligaments (connect bone to bone) and tendons (connect muscle to bone) are comprised of connective tissue that helps provide structural stability and allow for muscular contraction for skeletal movement. These movements occur when muscles contract across a joint, point of interaction between two bones.

The material presented in this thesis will focus primarily on the foot and shank of the lower limb. The foot is the region of the lower limb distal to the ankle joint composed of twenty-six bones and various ligaments and tendons articulating with one another to stabilize the lower limb. **Figure 2-2** shows these twenty-six bones of the foot are divided into three groups, the tarsal bones (rear foot), metatarsals (midfoot), and phalanges (forefoot; bones of the toes). The tarsal bones consist of the talus, calcaneus, navicular, cuboid, and three cuneiforms. There are five metatarsals in the midfoot numbered one to five from the medial to lateral portion of the foot, respectively. The phalanges are the bones of the toes where each toe has three phalanges (proximal, medial, and distal) except for the great toe which consists of only two phalanges.

The portion of the lower leg between the foot and thigh, composed of the tibia and fibula (**Figure 2-3**), is known as the “shank.” The tibia is the larger, weight-bearing bone on the medial aspect of the lower leg. The fibula is the smaller bone on the lateral aspect of the lower leg. The tibia and fibula are stabilized by connective tissue between the two bones known as the interosseous membrane. At the distal end of the tibia is the medial malleoli and at the distal end of the fibula is the lateral malleoli. The ankle joint is the

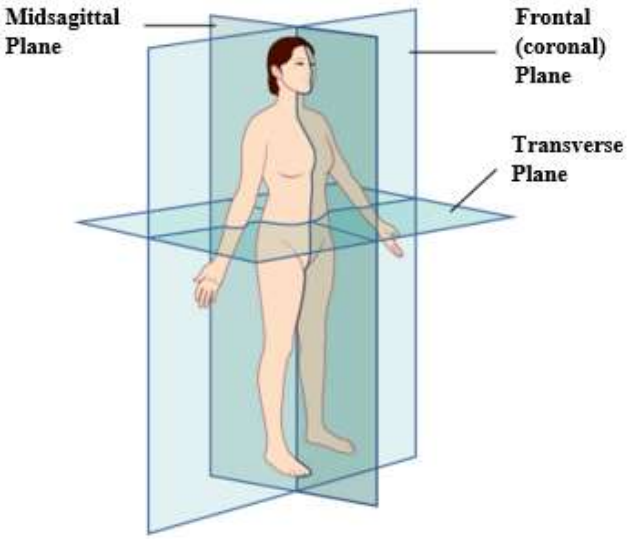

Figure 2-1. Anatomical Planes of the Body.
Reprinted with open access permission. Betts, J. G., Johnson, E., Wise, J. A., & Young, K. A. (2020). Planes of the Body. In Anatomy and Physiology: OpenStax. Retrieved from https://assets.openstax.org/oscms-prodcms/media/documents/AnatomyandPhysiology-OP.pdf on September 26, 2022 [18].

Figure 2-2. Bony Anatomical Structures of the Foot.
The cuneiforms, cuboid, and the navicular are collectively referred to as the tarsal bones
Reprinted with permissionVenkadesan, M., Yawar, A., Eng, C.M., Dias, M.A., Singh, D.K., Tommasini, S.M., Haims, A.H., Bandi, M.M., & Mandre, S. (2020). Stiffness of the human foot and evolution of the transverse arch. Nature, 579,104. https://www.nature.com/articles/s41586-020-2053-y [19].

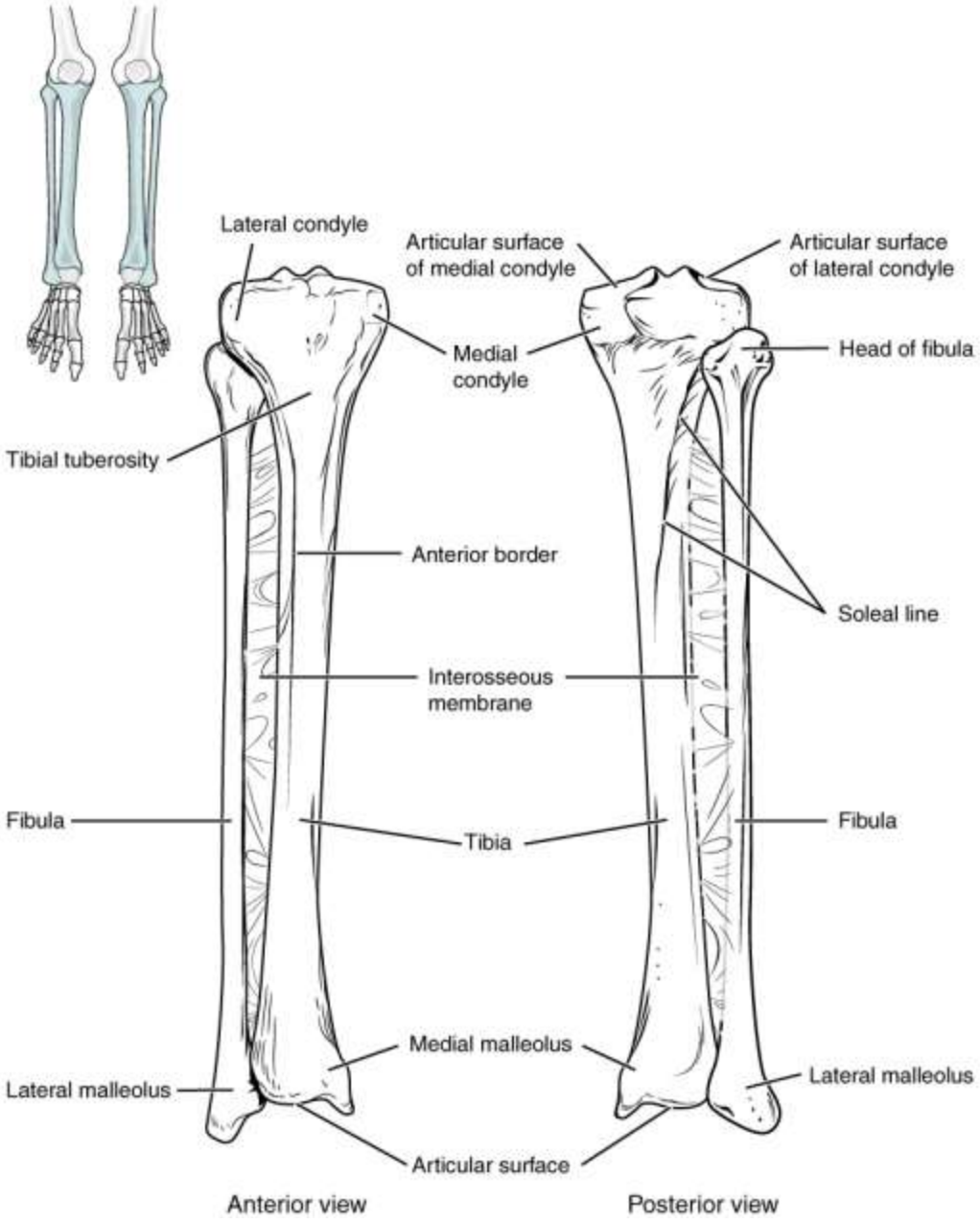

Figure 2-3. Tibia and Fibula Bone Anatomy.
Reprinted with open access permission. Betts, J. G., Johnson, E., Wise, J. A., & Young, K. A. (2020). Planes of the Body. In Anatomy and Physiology: OpenStax. Retrieved from https://assets.openstax.org/oscms-prodcms/media/documents/AnatomyandPhysiology-OP.pdf on September 26, 2022 [18].

region of the lower limb where the foot and shank interact with each other. various tendons and ligaments cross the ankle joint from the shank to the foot and help to stabilize the bony segments.

Working within the sagittal plane, the movements of the talocrural joint act as a hinge joint. Pointing the toes downward is known as plantarflexion. Pointing the toes upwards is known as dorsiflexion. The interaction between the distal tibia and fibula along with the talus forms the tibiotalar joint (**Figure 2-4**) which primarily functions in a uniaxial motion contributing to dorsi- and plantarflexion, however the internal and external rotation that occurs during dorsiflexion and plantarflexion, respectively, leads many individuals to suggest that this simultaneous motion occurs as a result of the oblique axis of the joint. [20]. Human anatomy varies between every individual; however, natural ankle range of motion during walking is a maximum of 30° in the sagittal plane (10° dorsiflexion, 20° plantarflexion) and approximately 35° in the frontal plane (23° inversion and 12° eversion) [20].

There are primarily three arches of the foot (**Figure 2-5**). Within the sagittal plane, there is the medial longitudinal arch (highest) located along the medial aspect of the foot, the lateral longitudinal arch (lowest) located along the lateral aspect of the foot, and the transverse arch. The longitudinal arches span between the posterior calcaneus to the metatarsal heads. The first, second, and third cuneiforms articulate with the first, second, and third metatarsals, respectively, while the cuboid articulates with the fourth and fifth metatarsals forming a lateral and medial column of the foot. This creates an arch within the transverse plane of the foot. These arches provide a curved structure of the foot that is more structurally stable and flexible enough to help dissipate the load as the foot is loaded with an individual's body weight during locomotion. The plantar fascia connects from the medial calcaneal tuberosity and inserts past the metatarsal heads, supporting and maintaining the arch of the foot during dynamic movements when extending onto the ball of the foot.

Human Locomotion

When an individual can move from one location to another through the repetitive motion of the foot striking the ground and progressing forward until the same foot leaves the ground, they are undergoing human locomotion (**Figure 2-6**). Human locomotion encompasses walking, running, swimming, jumping, etc. [21]. Normal human locomotion is divided into two phases during walking, stance phase (period from heel strike to toe off) and swing phase (period of time from toe off to heel strike). The stance phase is broken down into three sub-phases: initial double support (both feet in contact with the ground; one establishing heel strike, the other pushing off to propel the body forward), single limb stance (one foot is in contact with the ground, the other is swinging forward), second double support (the swinging foot has established heel contact; the previous foot is about to push off the ground, propelling the body forward). Stance phase constitutes roughly 60% of a single gait cycle. Once the foot has finished toe-off, it enters the swing phase which is also categorized into three sub-phases: initial swing (propelling

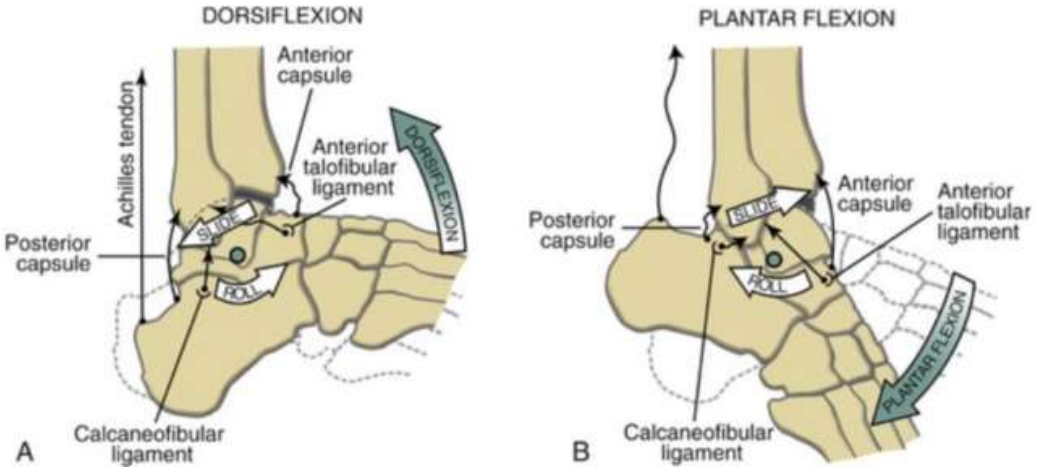

Figure 2-4. Interaction Between the Distal Tibia, Fibula, and Talus Forms the Tibiotalar Joint Acting as a Hinge.
Reprinted with permission. Neumann D. A. (2016). Kinesiology of the Musculoskeletal System: Foundations for Rehabilitation. Mosby, 3, 606. Retrieved from https://www.elsevier.com/books/kinesiology-of-the-musculoskeletal-system/neumann/978-0-323-28753-1 on November 1, 2022 [22].

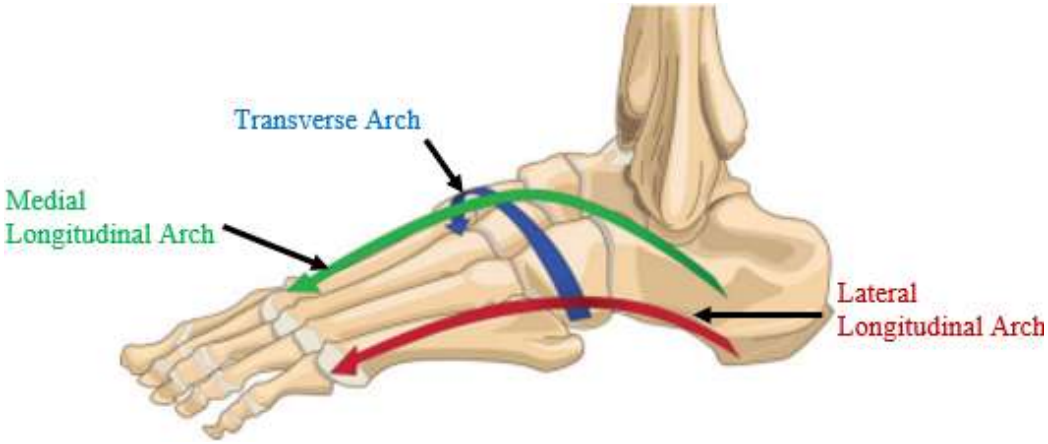

Figure 2-5. The Medial Longitudinal, Lateral Longitudinal, and Transverse Arches of the Foot.
Modified with permission. Flores, D.V., Gomez, C.M., Hernando, M.F., Davis, M.A., Pathria, M.N. (2019). Adult acquired flatfoot deformity: anatomy, biomechanics, staging, and imaging findings. RadioGraphics, 39, 1438. https://doi.org/10.1148/rg.2019190046 [23].

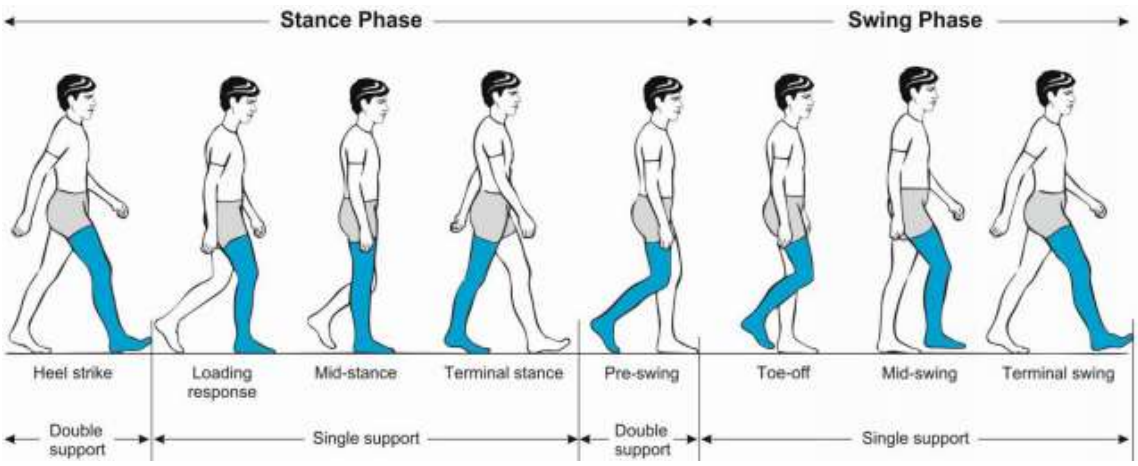

Figure 2-6. Different Phases of the Walking Gait Cycle.
Reprinted with open access permission. Pirker, W. & Katzenschlager, R. (2017). Gait disorders in adults and the elderly. The Central European Journal of Medicine, 129, 82. doi:10.1007/s00508-016-1096-4 [24].

the foot forward; acceleration), mid swing (foot is swinging forward), terminal swing (just before heel contact; deceleration). The swing phase consists roughly 40% of a single gait cycle.

Forces in Human Movement

Newton's third law states that for every applied force in nature, there is an equal and opposite reaction. During walking gait cycles, as an individual's heel strikes the ground and the foot is accepting the load, a force is applied to the walking surface and the surfaces pushes back against the body with an equal external force known as a ground reaction force (GRF). "These GRFs act on the foot creating a moment at the ankle joint which are resisted or controlled by muscle action" [21, p.6]. The internal forces produced by the muscles of the lower leg must overcome the external forces acting on the body. Typical GRF measures for walking fall within 1 to 1.2 units of body weight. This value is calculated by dividing the GRF by the individual's body weight.

Even though monitoring GRFs is a common practice in gait biomechanics, GRFs represent a small fraction of the overall internal force experienced by a structure within the body. However, the forces produced by the muscles that act on the bone structures is much greater than the external GRFs acting on the body, and the muscle forces can increase with stronger muscular contractions without increasing the GRF [25]. Using the tibia bone in running as an example, peak GRF occurs during load acceptance after initial foot contact, whereas the peak muscular contractive force occurs around midstance closer to when the runner is beginning to propel their body forward. The overall force acting on the tibia bone is the addition of the GRF and muscular force (**Figure 2-7)**. In walking and running, these loads can be anywhere between 5 to 10 units of body weight [25-27].

Bone Remodeling

In this thesis, the concepts of bone remodeling are discussed in relation to the mechanical properties of stress and strain, therefore it is important to understand the phases of bone remodeling, bone fatigue, and stress and strain. Bone remodeling occurs due to hormonal changes or mechanical stimuli and involves the removal of old bone (via osteoclasts) and synthesis of new, stronger bone (via osteoblasts). **Figure 2-8** provides an illustration of the bone remodeling process. The first phase of the remodeling process (Activation) occurs when the bone homeostasis is disrupted. This disruption can be a hormonal response or a mechanical stimuli response. From this response, osteoclast cells are differentiated and distributed to regions of the bone and will "secrete hydrogen ions and enzymes in particular cathepsin K so as to break down the bone matrix" [30, p.3-4]. The second phase (Resorption) follows where the pH of the bone matrix is lowered and digested leaving cavities within the bone [30]. Once this process is finished, osteoclasts cells undergo apoptosis (cell death) leading to phase three (Formation) where osteoblasts cells come in and begin to synthesis new bone. This process will continue until the synthesized bone mineralizes (calcifies), leading to phase 4, terminating the remodeling

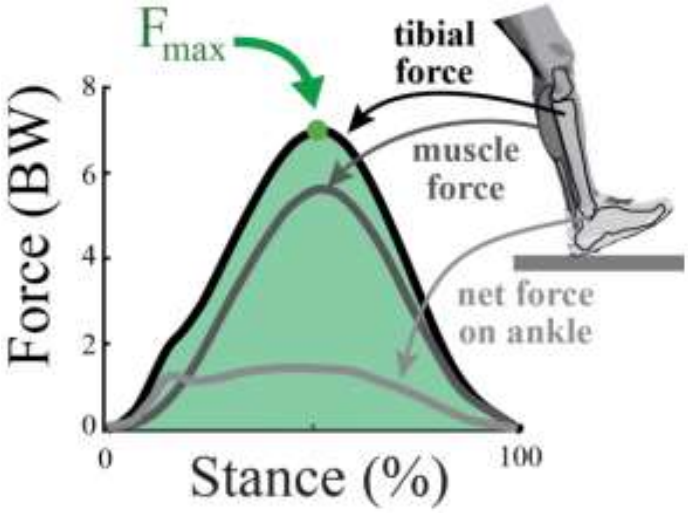

Figure 2-7. A Musculoskeletal Model Used Motion Capture and Ground Reaction Force Data to Calculate the Tibial Compressive Force.
Reprinted with permission. Matijevich, E. S., Scott, L. R., Volgyesi, P., Derry, K. H., & Zelik, K. E. (2020). Combining wearable sensor signals, machine learning and biomechanics to estimate tibial bone force and damage during running. Hum Mov Sci, 74, 102690. doi:10.1016/j.humov.2020.102690 [28].

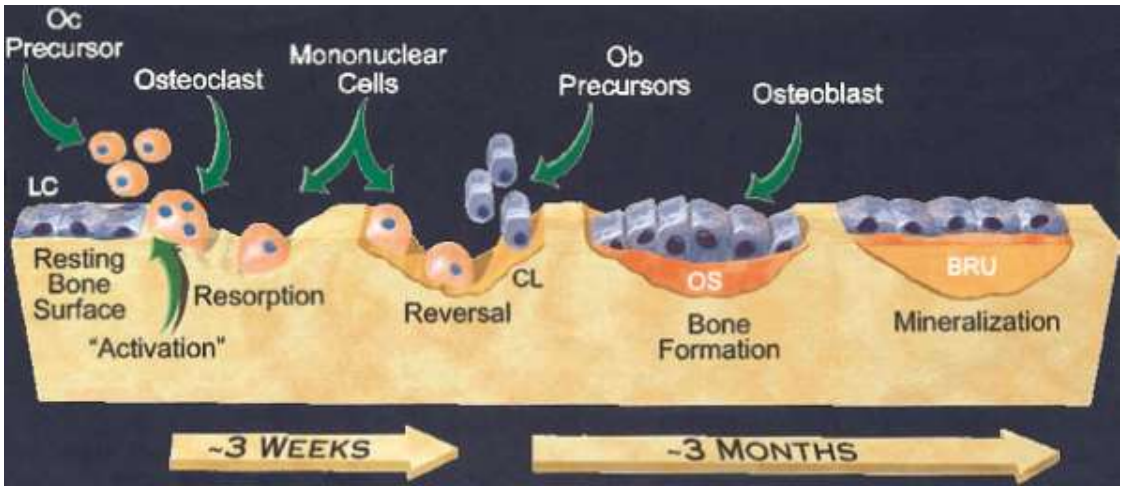

Figure 2-8. Overview of the Bone Remodeling Process.
Reprinted with permission. Rodan, G.A. (2003). The development and function of the skeleton and bone metastases. Cancer, 97(3), 728. doi:10.1002/cncr.11147 [29].

process [30]. This remodeling process helps to preserve the mechanical strength of bone. “Cortical bone turnover in the adult is at a rate of 2% - 3% per year. This [turnover] rate is adequate to maintain the biomechanical strength of bone” [30].

Stress and strain are fundamental concepts in bone biomechanics. When a force is applied across the cross-sectional area of the tibia, a compressive or axial stress is introduced that structurally deformations the bone. These two parameters help to define the mechanical properties of bone (**Figure 2-9**). Permanent damage occurs once the applied stress reaches the yield point of bone. Under cyclic loading conditions, the mechanical properties of bone fatigue over time, reducing the yield point when failure occurs. [2,3]. When provided with sufficient time to rest and recover, bone can remodel and adapt to the loading environment [31]. However, when the rate of bone damage outweighs the rate of recovery, under repeated loading, microcracks will propagate without any loss of stiffness until the last 10% of the cycle life where there is a rapid loss of stiffness leading to a fracture (**Figure 2-10**) [3,32-34]

Current Treatment Options for Tibial Stress Fractures

Walking boots were developed as a cost-effective alternative treatment option to plaster casts and provide patients with a means of removing the boot for hygiene purposes while aiding in pain reduction and functional movement [35]. Another benefit of a removeable walking boot is they can be removed for short periods of time to perform rehabilitative exercises designed to limit muscle atrophy and dysfunction to maintain ankle joint mobility.

General rehabilitation methods for handling stress fractures are split into two phases. Phase one (acute phase), requires a period of immobilization and reduced loads where rest, ice, compression, and elevation (RICE) is needed [8]. Pneumatic leg brace, crutches, or walking boot is used to limit the forces and manage the injured site to help promote bone healing. Any activities performed during this time should be pain-free, non-impact activities (i.e., swimming, cycling, water running) to help manage cardiovascular health. When, the patient is pain-free during non-impact activities, they can progress to the second phase where progressive loading begins. During this phase, so long as the individual is pain-free, they can progress from non- weight bearing to weight bearing activities, increasing bone loading, and incorporating proprioception and stretching exercises to assist with muscle function [8,9,36].

Dynamic Ankle Orthosis

The Dynamic Ankle Orthosis was originally designed as an alternative conservative treatment for ankle osteoarthritis [16] where the cartilage of the ankle joint and distal tibia bone degrades over time leading to increased joint stiffness and pain [37]. The device applies a distractive force across the ankle joint while retaining natural ankle

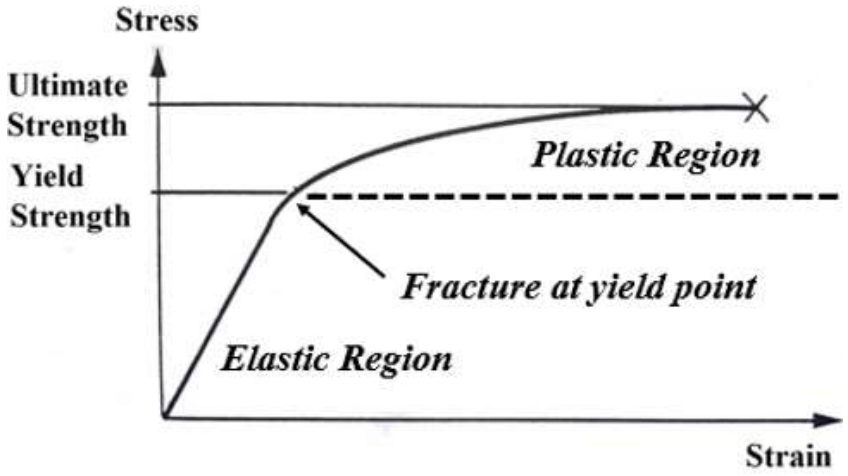

Figure 2-9. Measurements of Strength from the Stress Strain Curve.
Modified with permission. Turner, C. H., & Burr, D. B. (1993). Basic biomechanical measurements of bone: a tutorial. Bone, 14(4), 595-608. doi:10.1016/8756-3282(93)90081-k [3].

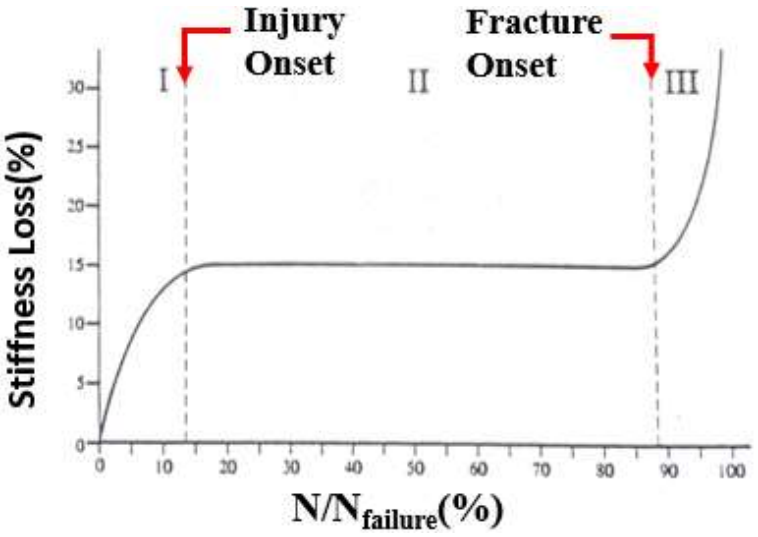

Figure 2-10. Change in Bone Stiffness During Fatigue.
Modified with permission. Turner, C. H., & Burr, D. B. (1993). Basic biomechanical measurements of bone: a tutorial. Bone, 14(4), 595-608. doi:10.1016/8756-3282(93)90081-k [3].

motion during level walking [16]. **Figure 2-11** shows the DAO brace is comprised of a calf sleeve, modified shoe, and two pneumatic cylinders. Ball joints connect the pneumatic (air) cylinders to the shoe and calf sleeve and allowed functional ranges of dorsiflexion and plantarflexion during walking activities. When the cylinders are pressurized, the distractive force is applied along the longitudinal axis of the tibia that reduced the load passing through the foot and ankle complex. The remaining internal forces still pass through the foot and ankle, and eventually the shoe to be absorbed by the ground [16]. Under static conditions, the DAO reduced longitudinal tibial loads by 11.3 to 30.5 percent [15]. During dynamic treadmill walking, the DAO reduced plantar pressure of toes 2 to 5 and the hallux by 12% and 24%, respectively, compared to an unbraced condition and standard of care Ankle Foot Orthosis (AFO) condition while retaining frontal and sagittal plane ankle motion [16].

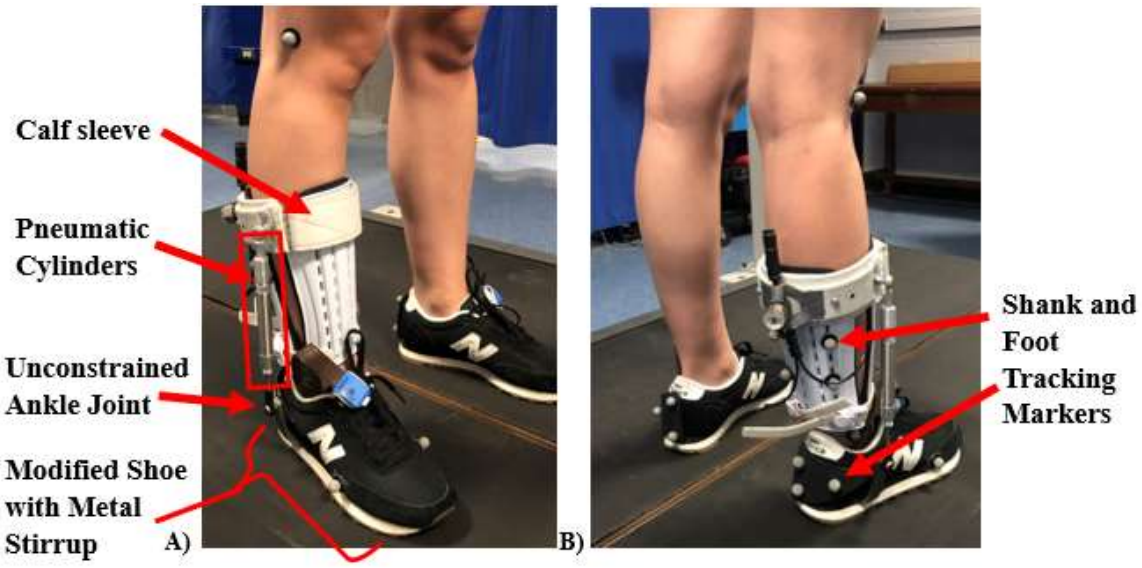

Figure 2-11. Participant Wearing the Dynamic Ankle Orthosis.
DAO: Dynamic Ankle Orthosis. A) Anterior – Lateral View and B) Posterior – Lateral View. Figures illustrate the different components of the DAO and the tracking markers used during data collection.

CHAPTER 3. STUDY 1: EFFECTS OF A DYNAMIC ANKLE ORTHOSIS TO REDUCE TIBIAL COMPRESSIVE FORCES DURING TREADMILL WALKING COMPARED TO A CLINICAL WALKING BOOT

Introduction

Running is a common form of exercise that has many health benefits but unfortunately, overuse injury rates and incidences are high among distance runners. The repetitive nature of running at submaximal levels causes the mechanical properties of bone to fatigue over time leading to increased strain and the development of micro-fractures [2,3]. When provided with sufficient time to rest, bone can remodel and adapt to the loading environment [31]. However, when the rate of bone damage outweighs the rate of repair, microcrack propagation can lead to stress fractures [3,32-34]. Tibial stress fractures (TSF) are a common overuse injury accounting for 21.9 – 69% of stress fracture incidence among runners [1,38] and 24 – 51.2% of stress fractures in military cadets [4, 39, 40]. TSF most commonly occur in the middle to distal third of the anterior tibia from rapid increases in physical activity or running exposure [41].

A period of reduced loading experienced at the injured site is often recommended following the initial diagnosis of a TSF [36]. Current standard of care consists of TSF patients wearing a walking boot to immobilize the lower limb during the recovery period. The severity of the stress fracture will often dictate the period of time the TSF patient will wear a boot. Even for low-risk stress fracture injuries that are generally treated with conservative methods compared to high-risk stress fracture injuries that require surgical treatment, patients are typically prescribed boot wear for 3 – 12 weeks, depending on the level of severity of the injury, before returning to running activities [4,9,36,42]. General rehabilitation methods for handling stress fractures are separated into two phases. Phase one (acute phase), requires a period of immobilization and reduced loading where rest, ice, compression, and elevation (RICE) is needed [8]. When the patient is pain-free, they can enter the second phase of rehab incorporating progressive loading [8,9,36]. Although walking boots are the current standard of care, there is no knowledge if, or how, they affect loading mechanics on the tibia.

Most studies on tibial stress fractures have focused on clinical outcomes [4,13,14] and do not examine the mechanical loading environment of bone when wearing a walking boot. Findings from studies focused on the biomechanics of walking boots found they provide a reduction in forefoot pressure, but conflicting evidence suggest they moderately reduce or increase heel pressure [10-12,43]. Walking boots also limit sagittal ankle motion causing reduced muscle activity which could, and generally does, lead to muscle atrophy of the gastrocnemius, soleus, and peroneal muscles [44-47]. Muscular atrophy contributes to prolonged rehabilitation time which delay return to training or competition in athletes. Further, Bailon-Plaza et al., studied fracture healing of sheep tibia under different loading and timing of mechanical stimulations, and determined the axial loading stiffness over a 100N load range divided by the average nodal displacement of the cortex [48]. They observed that moderate mechanical loading provides a positive

loading environment for quicker bone ossification and increased stiffness at the injured site compared to intact bone. By week 12, the stiffness of the stimulated bone group had reached 70 – 94% of the intact bone compared to half of the unstimulated bone group reaching 70 – 80% stiffness and the other half reaching 30-33% stiffness of the intact bone. Further, devices that allow appropriate mechanical loading of the tibia and minimize lower limb muscle atrophy during rehabilitation may help improve return to training or competition time in athletes or military personnel. Surprisingly, no studies have assessed the mechanical loading of the tibia in a walking boot, or in alternative rehabilitation devices, during daily walking activities.

A novel dynamic ankle orthosis (DAO), consisting of a calf sleeve, modified shoe, and two pneumatic cylinders (**Figure 3-1A**), was recently designed that applies a distractive force to offload the foot and ankle while also retaining natural ankle motion during level walking [16]. During treadmill walking when compared to a no brace condition, the DAO was able to significantly reduce peak plantar pressure under toes 2 – 5 by 12% and under the hallux by 24% while a double upright ankle foot orthosis increased peak plantar pressure under toes 2 – 5 and hallux by 14% and 6%, respectively [16]. A second study assessing the effects of acute DAO wear on perceived function and underfoot forces in symptomatic patients who have experienced mechanical foot and ankle pain symptoms found that the DAO moderately reduced vertical in-shoe force compared to a no brace condition during overground walking [17]. Although the DAO has been shown to reduce peak vertical in-shoe force while retaining natural ankle motion in healthy adults, its effectiveness to reduce the loading environment experienced by the tibia while walking remains unknown. The purpose of this study was to determine the biomechanical effects of a dynamic ankle orthosis on tibial bone loading and sagittal ankle motion compared to a standard-of-care walking boot in healthy individuals during treadmill walking. We hypothesized that the DAO would reduce the tibial compressive force and allow greater sagittal ankle motion compared to the walking boot.

Methods

Participants

A prior power analysis using an effect size f of 0.32 (from estimated Achille's tendon force between a walking boot and the DAO in preliminary analyses), alpha set to 0.05, and power of 0.8 for two within-subject repeated measurements suggested that a minimum of 18 participants were necessary to obtain the statistical effect size and power to test our hypotheses. Therefore 20 participants were recruited (10 men,10 women; 23 ± 2.4yrs; 1.7 ± 0.01m; 69.1 ± 11.4kg; 12.6 ± 0.02% static offloading) for this study. Inclusion criteria were participants between the ages of 18 to 40 years having a body mass below 90 kg (due to instrument limitations) and no lower limb injuries in the past 12 months. Participants were excluded if they had any chronic disorders or orthopedic conditions that could influence walking mechanics, or if they were pregnant at the time of the study. Participants were informed of all procedures and potential risks and signed a written consent form approved by the Institutional Review Board prior to data collection.

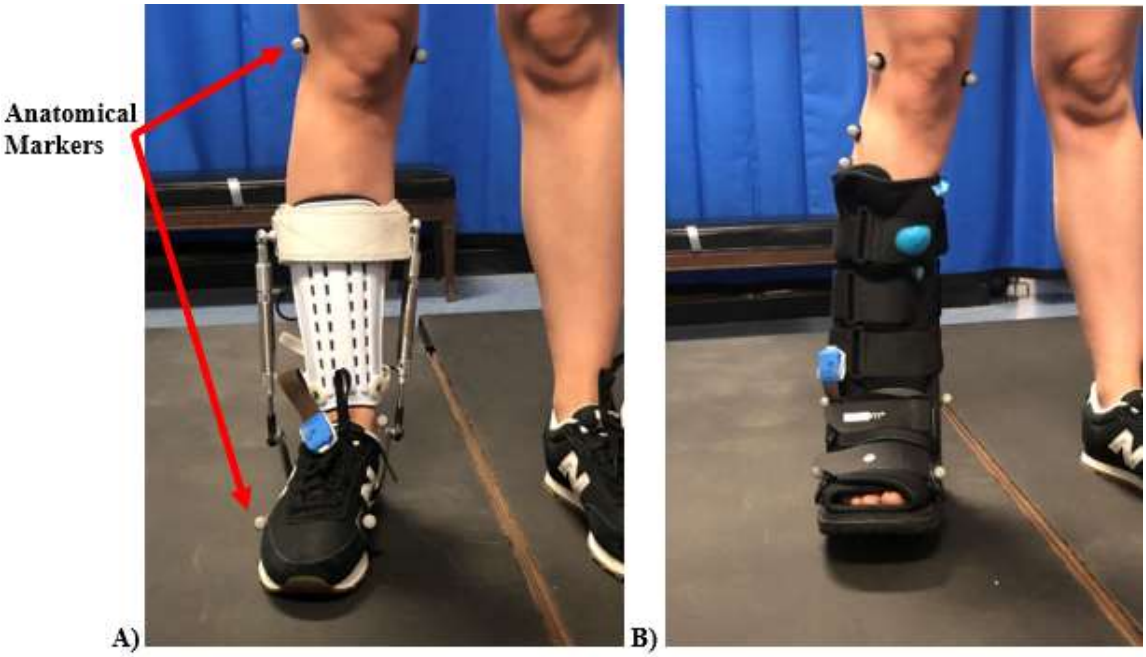

Figure 3-1. Brace Conditions Used for Testing During Treadmill Walking.
DAO: Dynamic Ankle Orthosis. A) DAO – Front View and B) Walking Boot – Front View. Anatomical markers were positioned at the first and fifth metatarsal heads, medial and lateral malleoli, and medial and lateral epicondyles to define segment lengths and joint centers

Orthosis Conditions

Two brace conditions were tested: the DAO (0.78 ± 0.12kg) and a standard of care walking boot (Össur FormFit Walker Air; 0.5 ± 0.06kg; **Figure 3-1B** and **Figure B-1**). The shoe used for the DAO conditions (model 501, New Balance, Boston, MA) was modified with a metal stirrup and plate embedded in the sole of the shoe which provided connection to the upper orthosis components. Previous validation testing showed that the DAO provided comparable ranges of movement to the intact ankle joint allowing for at least 10° of dorsiflexion, 15° of plantarflexion, and at least 10° of inversion and eversion [16]. In a previous study with the DAO, a targeted offloading of at least 10% of the participants body weight was recommended by orthotists regarding the level of offloading necessary to achieve pain reduction [16]. Equipment specifications are listed in **Appendix A** (**Table A-1**). In this study, the DAO was activated to offloaded 10% bodyweight based on the static protocol outlined below. The heel portion of the foam material of the walking boot was removed to secure reflective markers on the heel to track foot motion during testing (**Figure 3-2** and **Figure B-2**).

Experimental Protocol

The two brace conditions were randomized and worn on the participants right limb. For the DAO condition, static offloading (10% bodyweight target) was determined during standing by taking the percent difference in the insole force reading before and after pressurizing the pneumatic cylinders. The static protocol was performed five times per participant to ensure proper offloading. Each brace condition was worn for 5 to 10 minutes during both standing and walking prior to data collection to provide a period of brace familiarization.

Individual retro-reflective markers were positioned on the first and fifth metatarsal heads, medial and lateral malleoli, and medial and lateral femoral epicondyles to define segment dimensions, joint coordinate systems, and to establish a relationship between joint centers and anatomical tracking markers. Clusters of tracking markers were placed on the right rearfoot and shank in different positions for each brace condition to track each segment. For the DAO condition, tracking markers were positioned on the posterior region of the shank on the DAO calf sleeve component. A heel cluster of three tracking markers rigidly attached to a thermoplastic plate was securely positioned on the posterior aspect of the shoe. For the walking boot condition, a cluster of four tracking markers were positioned at the posterior-lateral and proximal portion of the skank above the walking boot brace. An 8-camera 3D motion capture software with Qualisys Track Manager software (240Hz, Qualisys AB, Gothenburg, Sweden) captured 3D kinematic data while a force instrumented split-belt treadmill (1200Hz, Bertec, Inc, USA) collected 3D GRF data and a wireless vertical force-sensing insole (100Hz, loadsol, Novel, St. Paul, MN) was inserted into the braced shoe to capture in-shoe vertical reaction force time-series data during treadmill walking. Insole force data were calibrated using the manufacturer procedure before testing in each brace condition. Following a one-second standing calibration trial, anatomical markers were removed prior to treadmill walking.

Figure 3-2. Foam Material Removed from Walking Boot to Expose the Heel to Track Foot Motion.

Participants walked on the 3D force treadmill at 1.0 m/s for five minutes to become acclimated to each brace condition prior to data collection. After walking on the force treadmill for an additional two minutes, 3D kinematic, kinetic, and insole vertical force data were captured for thirty seconds (**Figure B-3**). At the start of each walking condition, participants took a forceful step with their right foot on the treadmill to identify an instant in time, detected from all three instruments, to synchronize all data. Participants were allowed to rest for at least five minutes, or until they felt well rested, between brace conditions to minimize fatigue effects. From the thirty seconds worth of data captured, ten sequential steps were used from each brace condition for data analysis. Following each testing trial participants rated their comfort level in each brace condition using a custom visual analog scale. Comfort was rated with 0: "very comfortable," 2: "comfortable," 4: "moderately comfortable," 6: "moderately uncomfortable," 8: "Uncomfortable," 10: "extremely uncomfortable." (**Figure B-4**)

Data Analysis

3D kinematic, insole force, and GRF data were processed and analyzed for ten sequential steps using Visual 3D software (C-Motion, Germantown, MD; **Figure B-5**). The raw kinematic, insole force, and GRF data were interpolated to fill data gaps no greater than ten frames and filtered using a Butterworth low-pass filter with cut-off frequencies of 6Hz, 15Hz, and 15Hz respectively. Right-hand rule with Cardan rotational sequence (x-y-z) was used for 3D angular kinematic computations, where x represents rotations about the mediolateral axis, y represents the rotation about the anteroposterior axis, and z represents the rotation about the vertical axis of the distal segment. Sagittal plane ankle kinematics were resolved in the shank coordinate system and all variables were analyzed during the stance phase of gait. Insole force data were processed using MATLAB (MathWorks, Natick, MA). A vertical force threshold of 25N was used to define heel contact and toe-off for both the insole force and GRF data. 3D kinematic, treadmill kinetic, and insole force data were used to calculate the moment acting about the ankle joint at time of peak plantarflexor moment.

The 3D kinematic and treadmill GRF data were correlated with the time point of the insole vertical force (VRF_z) data to determine the net ankle moment at peak plantarflexor moment for inverse dynamic calculations (**Figure 3-3**). Since the force treadmill did not account for any reduction in the vertical GRF component due to the offloading effect of the DAO, the vertical GRF vector was replaced with VRF_z. It is also important to note that the information from the instrumented force treadmill and force-sensing insole provide different force vector data. The instrumented treadmill provided the resultant GRF while the force sensing insole provided the vertical GRF component. An image of the participants lateral right foot, from the lateral malleolus to Achilles tendon was taken and uploaded to ImageJ (National Institute of Health, University of Wisconsin). From this image, the anteroposterior distance between the lateral malleolus and the superficial surface of the Achilles tendon was determined to represent the sagittal plane Achilles tendon moment arm (d_{AT}) to the ankle joint (**Figure 3-4**). Variables used in the calculations (**Table C-1**) include the moment about the ankle, M_A, moment of

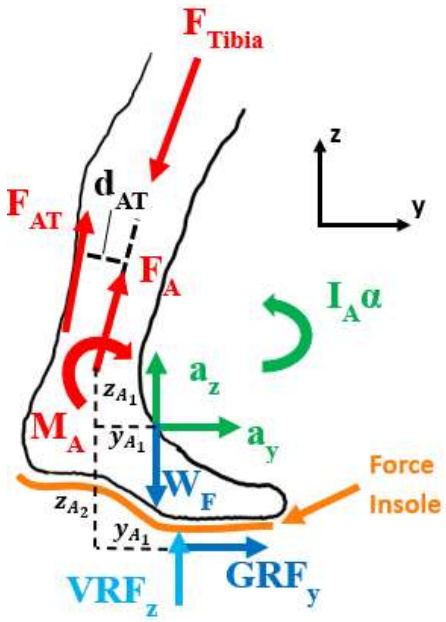

Figure 3-3. Free Body Diagram of Tibial Force Algorithm.

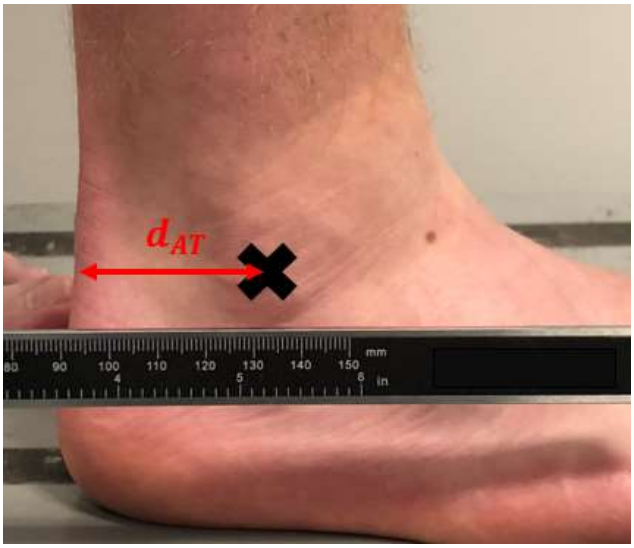

Figure 3-4. Example of Participant Foot Determining the Achilles Tendon Moment Arm.
d_{AT} is the Achilles tendon moment arm between the Lateral Malleoli and Achilles Tendon.

inertia about the ankle, I_A, angular acceleration, α, mass of the foot, M_F, linear acceleration, ay, linear acceleration moment arm, z_{A1}, vertical acceleration, a_z, vertical acceleration moment arm, y_{A1}, VRF_z moment arm, y_{A2}, propulsive GRF, GRF_y propulsive force moment arm, $z_{A1} + z_{A2}$ and gravity, g, as seen in **Equation 3-1**.

$$M_A = I_A\alpha - [(m_F * a_y) * z_{A_1}] - [(m_F * a_z) * y_{A_1}] - (VRF_z * y_{A_2}) - [GRF_y * (z_{A_1} + z_{A_2})] + [(m_F * g) * y_{A_1}] \quad \textbf{(Eq. 3-1)}$$

$$F_{AT} = \frac{M_A}{d_{AT}} \quad \textbf{(Eq. 3-2)}$$

$$F_A = \frac{F_z'}{\cos(\beta)} \quad \textbf{(Eq. 3-3)}$$

$$F_{tibia} = F_{AT} + F_A \quad \textbf{(Eq. 3-4)}$$

Achilles tendon force, F_{AT}, represents the muscle forces acting on the tibia. F_z' represents the summation of the vertical forces acting on the tibia (i.e., equal, and opposite to the summation of forces at the ankle, F_z) at angle β (angle of tibia at peak plantarflexor moment) and used to obtain the reaction force at the ankle, FA, acting along the longitudinal axis of the tibia. The peak compressive force, F_{tibia}, acting on the tibia was the addition of the ankle reaction force, F_A, and muscular forces, F_{AT} [27,28]. Peak plantarflexor moment was chosen as the specific time of interest because it is the point in stance phase, at the start of push-off, where the calf muscles are most involved in assisting with propelling the body forward [49]. Sagittal plane ankle excursion was defined by the period following heel contact to peak dorsiflexion after mid stance. Vertical impulse was determined as the area under the force time interval from the instrumented treadmill. Stance time and step length were measured during gait. The percent offloading provided by the DAO compared to the walking boot was determined by taking the difference between the peak force in the DAO, $Force_{DAO}$, and the peak force in the waking boot, $Force_{WB}$, divided by the peak force in the walking boot (**Equation 3-5)**.

$$\%\, offloading = \frac{Force_{WB} - Force_{DAO}}{Force_{WB}} \times 100 \quad \textbf{(Eq. 3-5)}$$

Statistical Analysis

A Shapiro-Wilk test was used to assess normality of the data per condition for each dependent variable. A paired t-test was used to determine brace effect for all dependent variables that passed normality. Cohen's d effect size was determined to assess the effect size for differences between dependent variables (i.e., small: $d < 0.2$, medium: $0.2 \leq d < 0.8$, large: $d \geq 0.8$). Step length, cadence, and brace comfort score failed normality (i.e., nonparametric), therefore, when normality was not confirmed, a Wilcoxon Sign Rank test was used to compare means. Effect size was determined to assess the effect size for differences between dependent variables (i.e., small: $d < 0.06$, medium: $0.06 \leq d < 0.14$, large: $d \geq 0.14$). A significance level of $p < 0.05$ was used for all tests.

Results

Brace effects were apparent in the DAO compared to the walking boot (**Table 3-1**) at time of peak plantar flexor moment. VRFz normalized to one hundred percent of stance phase can be found in **Appendix C** (**Figure C-1**). Significant difference in the peak tibial compressive force (10.9%, **Figure 3-5**) and Achilles tendon force (12.0%; **Figure 3-6**) were moderately lower in the DAO compared to the walking boot (**Table 3-1**). 55 percent of the participants experienced reduced peak tibial compressive when wearing the DAO compared to the walking boot (**Figure C-2**). Sagittal plane ankle motion (**Figure 3-7**) from during stance phase was reduced by 54.9% wearing the walking boot compared to the DAO (**Table 3-1**). The DAO demonstrated a longer stance time compared to the walking boot (**Table 3-2**). Vertical impulse (**Table 3-1**), and step length, cadence, and comfort rating (**Table 3-2**) were not significantly different between brace conditions.

Discussion

The overall goal of this study was to compare the effects of a dynamic ankle orthosis on lower extremity loading biomechanics during treadmill walking compared to a standard of care walking boot on young healthy adults. At peak plantarflexor moment, there was no difference in the VRFz reported by the force sensing insoles between the DAO and walking boot. It should be noted that there is a difference in the moment arm lengths between the walking boot and DAO (**Table C-1**). The shallow rocker sole and rigid design of the walking boot created a greater moment arm between the VRFz and ankle joint (**Figure 3-8**) which contributed to less dorsiflexion during the latter portion of the stance phase and resulted in a greater external moment at the ankle compared to the DAO. On the other hand, the DAO had a shorter forefoot rocker point (and moment arm) compared to the walking boot, and the unconstrained ankle joint of the DAO allowed the participant to raise their heel and pivoted about the metatarsal joint during the second half of stance which further reduced the horizontal distance between the vertical reaction force and ankle joint. The shorter moment arm with the DAO and corresponding external moment at the ankle moderately reduced ($d = 0.52$) the plantarflexor muscle forces at the Achilles tendon by 12% compared to the walking boot. This reduced Achilles tendon force associated with the DAO could potentially benefit individuals who have suffered an Achilles injury, especially since there is no current gold standard of treatment for Achilles injuries such as Achilles tendonitis [50].

Since the axial loading on the tibia primarily comes from the AT, the reduced Achilles tendon force with the DAO (**Equation 3-4**) resulted in a moderate reduction ($d = 0.48$) of the tibial compressive force by 10.5% compared to a walking boot at time of peak plantarflexor moment. This finding supports our first hypothesis that the DAO moderately reduced the tibial compressive force and further confirms that the recommended DAO offload setting of 10% was sufficient to create a significant difference in the amount of tibial force reduction (i.e., 10.5%). Of future interest is

Table 3-1. Kinetics and Kinematics in Each Brace Condition During Treadmill Walking.

Variables	DAO	Walking Boot	*P* Value	Effect Size (*d*)
Peak Tibial Compressive Force (BW)[a]	6.8 ± 1.4*	7.6 ± 2.2	0.022	0.48
Achilles Tendon Force (BW)[a]	5.8 ± 1.3*	6.6 ± 2.0	0.016	0.52
Ankle ROM (deg)[a]	29.2 ± 3.0*	13.2 ± 4.1	< 0.001	3.19
Vertical Impulse (N*s)	420.2 ± 76.0	414.1 ± 73.1	0.075	0.34

Mean ± Standard Deviation; DAO: Dynamic Ankle Orthosis. BW: Body Weight. ROM: range of motion. [a] Brace effect ($p < 0.05$). * Denotes significant difference from walking boot. Effect size: small effect = $d < 0.2$, medium effect = $0.2 \leq d < 0.8$, large effect = $d \geq 0.8$.

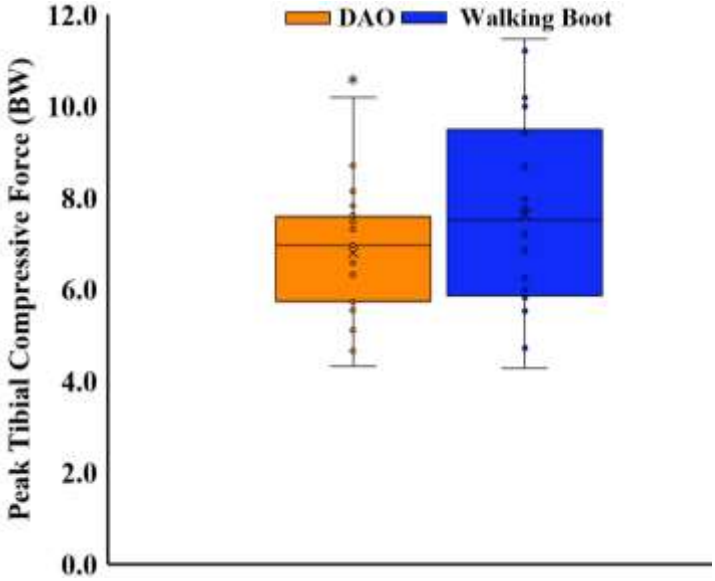

Figure 3-5. Peak Tibial Compressive Force (BW) at Peak Plantarflexor Moment During Treadmill Walking for the Right Limb in the Two Brace Conditions.
DAO: Dynamic Ankle Orthosis. BW: Body Weight. * Denotes significant difference from walking boot.

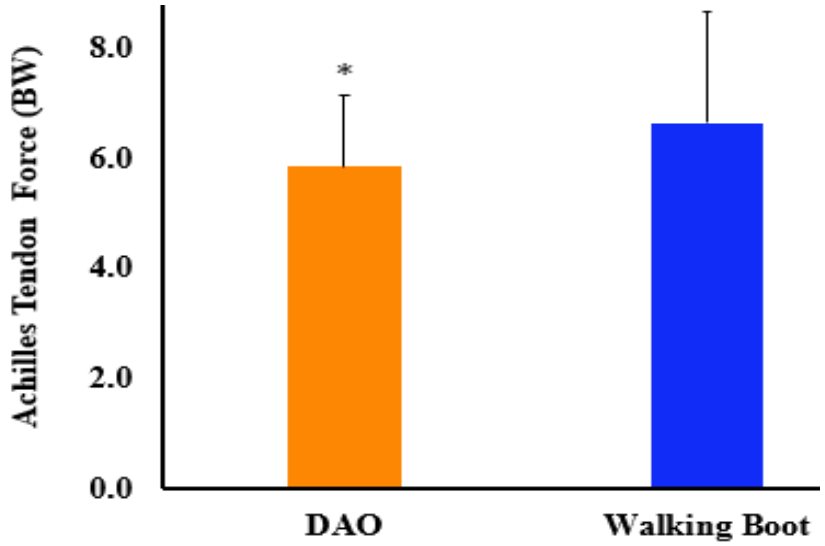

Figure 3-6. Achilles Tendon Force (BW) at Peak Plantarflexor Moment During Treadmill Walking for the Right Limb in the Two Brace Conditions.
DAO: Dynamic Ankle Orthosis. BW: Body Weight. * Denotes significant difference from walking boot.

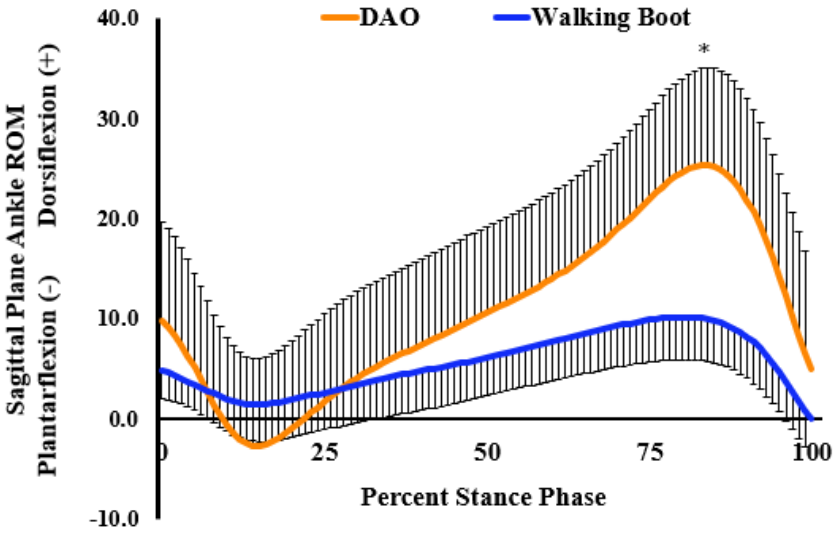

Figure 3-7. Sagittal Plane Ankle Joint Curves During Treadmill Walking for the Right Limb in the Two Brace Conditions.
DAO: Dynamic Ankle Orthosis. ROM: range of motion. * Denotes significant difference from walking boot.

Table 3-2. Spatio-Temporal Variables in Each Brace Condition During Set Treadmill Walking Speed.

Variables	DAO	Walking Boot	*P* Value	Effect Size (*d*)
Stance Time (s)[a]	0.77 ± 0.04*	0.74 ± 0.04	< 0.001	1.07
Step Length (m)	0.58 ± 0.05	0.57 ± 0.03	0.198	0.20
Cadence (steps/min)	105.18 ± 11.53	104.95 ± 5.99	0.422	0.13
Brace Comfort Scores	3.90 ± 2.59	4.95 ± 2.67	0.108	0.29

Mean ± Standard Deviation; DAO: Dynamic Ankle Orthosis. ROM: range of motion. [a] Brace effect ($p < 0.05$). * Denotes significant difference from walking boot. statistical analysis for step length and cadence were performed using a Wilcoxon sign rank test. Effect size: small effect = $d < 0.2$, medium effect = $0.2 \leq d < 0.8$, large effect = $d \geq 0.8$; Brace comfort scores: 0 = very comfortable, 10 = very uncomfortable.

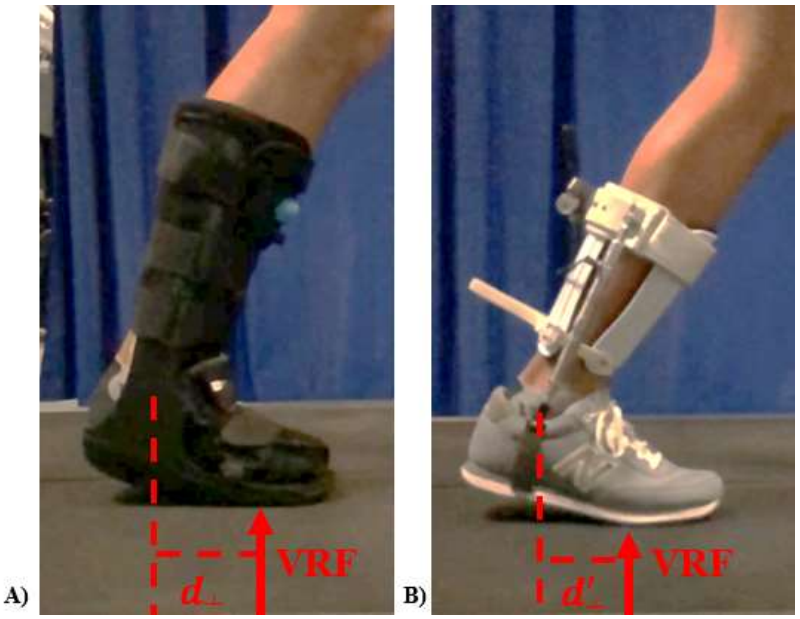

Figure 3-8. Increased Moment Arm When Wearing the Walking Boot.

confirming if the degree of offloading on the tibia provided by the DAO during a post tibial fracture recovery phase would enhance bone repair rather than bone damage.

The Achilles tendon loads determined in this study were comparable to other findings in the literature [26,51] (**Figure 3-9**). Hullfish et al. observed Achilles tendon loads of 2 BW compared to our results of 5.8 BW and 6.6 BW in the DAO and walking boot, respectively. Hullfish et al. (2020) developed a simplified protocol to quantify the load at the Achilles tendon using Loadsol insole vertical force data and a load cell attached to the inline of the posterior strut of a walking boot but did not measure ankle excursion. Their assumption that the ankle remained fixed in the walking boot and did not allow for any ankle movement created an over constrained system that negated any Achilles tendon involvement which may have led to a lower estimation of the Achilles tendon loading. Our model used a motion capture system and found the walking boot allowed some ankle joint movement (**Figure 3-7**). Some discrepancies exist on where the moment arm length was measured from that could explain the larger differences in the Achilles tendon force values. Our moment arm of 3.1cm was measure relative to the lateral malleoli, while Hullfish et al. (2020) reference other studies (citing 5.4cm) [52,53] as measured from the medial malleoli or midpoint between the lateral and medial malleoli.

Figure 3-10 provides a comparison of our tibial force values with other biomechanical studies [25-27] for walking and running. In the walking study by Meardon et al. (2021), the peak tibial bone loads for a group of recreational runners were 5000N (6.36 BW) and 3800N (6.65 BW) in men and women, respectively and were very similar to our findings. Scott & Winter (1990) developed a mathematical model to predict the loads at chronic injury sites during running. They observed an average peak tibial compressive force of 12.32 BW during stance phase. As one would expect, the peak tibia loads during running were greater than our measured values for walking.

The greater sagittal plane ankle excursion provided by the DAO from heel contact to peak dorsiflexion after mid stance supports the second hypothesis. Similarly, the walking boot significantly reduced sagittal ankle motion during stance phase by 54.9%. This loss of ankle motion can limit muscle activity and contribute to muscle atrophy in the gastrocnemius, soleus, and peroneal muscles [44-47]. Nahm et al. (2019) observed that participants experienced between 3 – 8° of sagittal tibiotalar motion while wearing the different walking boot conditions compared to a regular shoe. Zhang et al. (2006) observed between 5 – 7° of sagittal ankle excursion in individuals wearing short-leg walking boots during walking. While the walking boot used in this study provided slightly greater range of ankle of motion (13.2°), it remains unknown if muscle atrophy would occur during extended wear; in particular, during the recovery phase of a post tibial stress fracture. When an athlete is cleared to remove the walking boot, additional time is required to re-acclimate the bone and muscle tissue to the loading environment. On the other hand, the DAO provided near natural sagittal plane ankle motion of 29° [56, 57]. This increased ROM at the ankle joint can serve to provide more involvement of the plantar flexor muscles, thereby minimizing the effects of muscle atrophy that typically occurs when wearing a walking boot and allowing athletes a quicker return to sport.

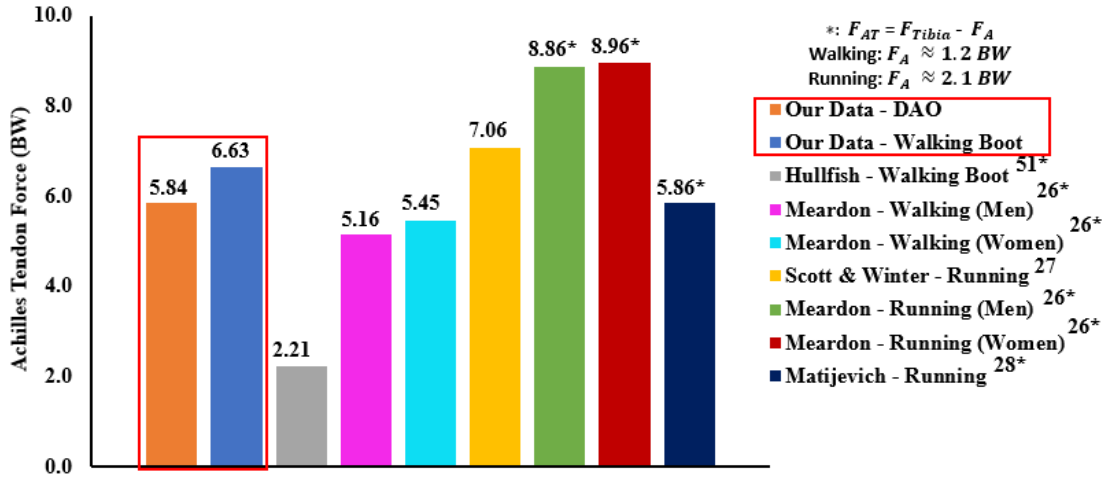

Figure 3-9. Achilles Tendon Force (BW) from the Current Study Compared to Previous Literature.
DAO: Dynamic Ankle Orthosis. BW: Body Weight. * Study only provided the tibial compressive load. A typical ground reaction force for walking or running respectively was subtracted from the tibial compressive force to provide an estimate of the Achilles Tendon Force from previous studies.

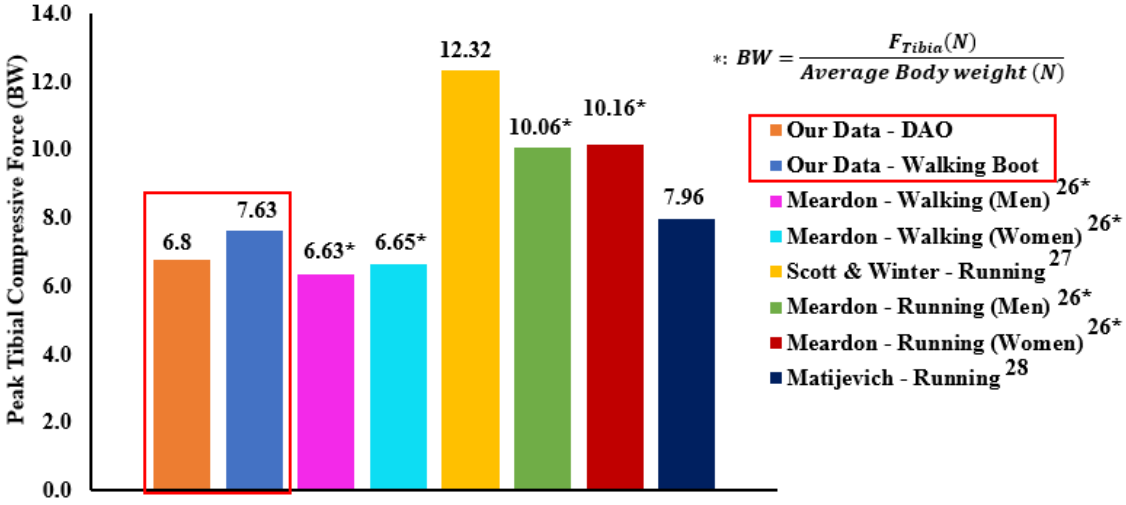

Figure 3-10. Peak Tibial Compressive Force (BW) from the Current Study Compared to Previous Literature.
DAO: Dynamic Ankle Orthosis. BW: Body Weight. * The tibial compressive force was only provided in newtons. The tibial compressive force was divided by the participant average body weight to provide an estimate in units of body weight.

The results of this study are limited to acute brace wear since participants were only allowed 5 – 10 minutes to become acclimated to the brace condition. To understand the long-term effects of the DAO compared to a walking boot, a clinical study where patients wear either brace condition over multiple weeks would need to be conducted. Brace sizes were limited to three options for the DAO (small, medium, and large) and two options for the walking boot (medium and large). Any brace adjustments were limited to what was feasible between the different brace sizes within the laboratory setting rather than creating patient specific customized braces. Peak impact and push-off forces have been shown to differ between overground and treadmill walking when wearing the DAO [17]. In this study, treadmill walking was chosen to control participant walking speed during testing and therefore, current findings may not be generalizable to overground conditions.

Conclusion

The findings from this study indicated that the DAO moderately reduced tibial compressive force and allowed more sagittal ankle motion during treadmill walking compared to a clinical walking boot. Conversely, a clinical walking boot restricted ankle mobility by more than 50% and significantly increased Achilles tendon and tibial compressive forces during treadmill walking. Future studies will explore the effects of increasing the amount of DAO offload and comparing the long-term effects of DAO wear in a tibial stress fracture population. With extended DAO wear, bone union may occur at a faster rate and patients may experience reduced muscle atrophy allowing athletes to return to their sport sooner.

CHAPTER 4. STUDY 2: BIOMECHANICAL ANALYSIS OF A DYNAMIC ANKLE ORTHOSIS TO REDUCE TIBIAL BONE STRAIN AND AXIAL LOADS COMPARED TO A CLINICAL WALKING BOOT

Introduction

The most common treatment for tibial stress fractures is use of a walking boot that serves to immobilize the ankle joint and stabilize the lower limb and foot to aid in the healing process. However, the effects of a walking boot on tibial bone strain and mechanical loading of the lower leg remains unknown. As shown in the previous chapter, the use of force platforms or wearable sensors (i.e., force insoles, motion capture, and accelerometers) has become a practical non-invasive means of determining the load experienced by the tibia due to ground reaction forces and muscular contribution by utilizing inverse dynamics [26,58,59]. While this is the current standard, in reality, the physiological response of bone, varies between individuals and has an impact on the strain magnitude and strain rate of the bone. Past researchers pioneered bone strain measurements by performing *in vivo* experiments where specific sites of an individual's tibia were surgically exposed, and a strain gauge was attached to capture physiological strain responses under various recreational activities [60-62]. Due to the invasive nature of measuring tibial strain *in vivo*, most tibial bone strain measurement studies were kept to small sample sizes [60,62,63].

The mechanical strain experienced by the tibial bone while wearing a walking boot is not documented. To the best of my knowledge, the closest examination of bone strain in a brace design was a study using a dynamic gait replicator to simulate stance phase in a cadaver model while wearing a custom and semi-custom rigid orthoses to analyze second metatarsal strain magnitude and strain rate [64]. Compared to a no brace condition, wearing the orthotics provided a small to moderate reduction for compressive, tensile, and sheer strain and strain rates during gait simulation. It is important that the bone strain is reduced within a clinical walking boot, otherwise the bone is potentially at risk of delayed bone union, delaying return to physical activity or increasing the likelihood of surgical intervention [65-67].

Based on bone mechanics theory (**Chapter 1**), injury onset, or permanent deformation, of bone can occur when the load reaches the yield point (**Figure 2-6**). However, with repetitive loading, the mechanical properties of bone will fatigue over time allowing for the injury onset to occur at a threshold below the yield point (**Figure 4-1**). Repeated loading above the injury onset threshold causes microcracks to form that will propagate without any loss of stiffness, eventually leading to a rapid loss of stiffness in the last 10% of the cycle life, leading to a fracture. Generally, prior to the onset of a fracture, when the rate of repair outweighs the rate of bone damage, bone is able to adapt to its loading environment (**Chapter 1**). However, when the rate of damage starts to outweigh the rate of repair, microcracks propagate into stress fractures. It is our suggestion that by reducing the loads and strain on the tibia that there might be a "safe

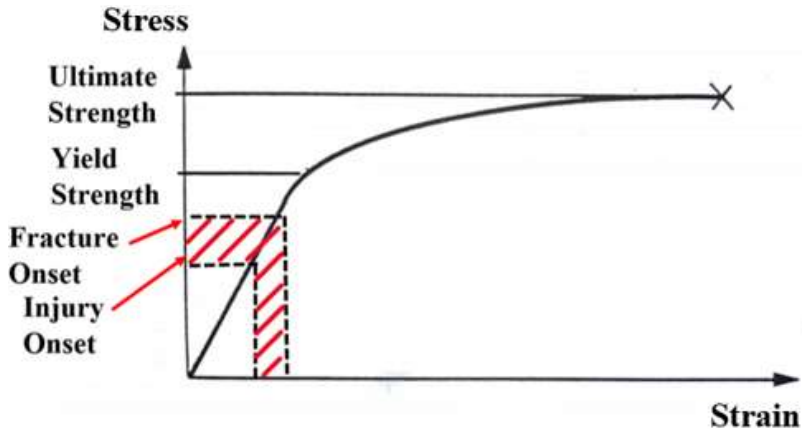

Figure 4-1. Measurements of Strength from the Stress-Strain Curve to Illustrate Threshold for Injury Onset and Initiation of a Fracture.
The red region indicates the stress/strain when under repetitive loading, the mechanical properties of bone will fatigue over time allowing for the injury onset to occur at a threshold below the yield point. Modified with permission. Turner, C. H., & Burr, D. B. (1993). Basic biomechanical measurements of bone: a tutorial. Bone, 14(4), 595-608. doi:10.1016/8756-3282(93)90081-k [3].

zone" below the tibial stress injury (TSI) threshold that an individual can operate at during the recovery period to help promote bone remodeling without further inducing bone damage (**Figure 4-2**).

Based on the previous treadmill walking study (**Chapter 3**), past validation testing, and walking assessment of the DAO [15-17], there is potential for the DAO to function as an alternative rehab method to control the mechanical loads acting on the tibia while providing increased ankle mobility to reduce muscle atrophy, and potentially shorten the recovery period. Therefore, the purpose of this study was to determine the offloading effects of the DAO on tibial bone strain and vertical reaction force measurements compared to a standard of care walking boot in a human cadaver model. We hypothesized 1) the DAO will reduce the strain magnitude and strain rate at the distal and midshaft tibia compared to a walking boot, 2) there will be an equivalent percent reduction in strain along with the percent reduction in the vertical reaction force from the instrumented force insoles and 3) there will be a moderate correlation between the tibial strain and vertical force measurements under uniaxial loading.

Methods

Specimens

Three fresh frozen cadaver legs (2 males, 1 female; 56 ± 19.5yrs; 5.44 ± 0.51kg) spanning from the mid femur to toes, were procured to test in a robotic testing platform. Only the right limb was procured due to the shoe design of the DAO brace attachment. Each specimen was imaged under a fluoroscopy machine to visually assess for any structural deformities or abnormalities. No specimen was found to have any deformities or abnormalities and therefore, no additional surgery was needed.

Specimen Storage

Prior to inserting into the freezer, each specimen was sprayed with saline and wrapped within cotton surgical pads to help keep the tissue healthy and prevent the tissue from drying out. Each specimen was placed in a plastic biohazard bag and given a specific label for identification. Each specimen was thawed in a refrigerator for at least 48 – 72hrs prior to experimental testing.

Dissection and Potting

Each leg specimen obtained was cut at the mid femur. The quadricep and hamstring muscles, along with all soft tissue of the thigh, were removed to expose the femur. Due to limited testing space available within the robotic testing platform, the femur of each specimen was trimmed until ~3 – 3.5in of the femur remained. The

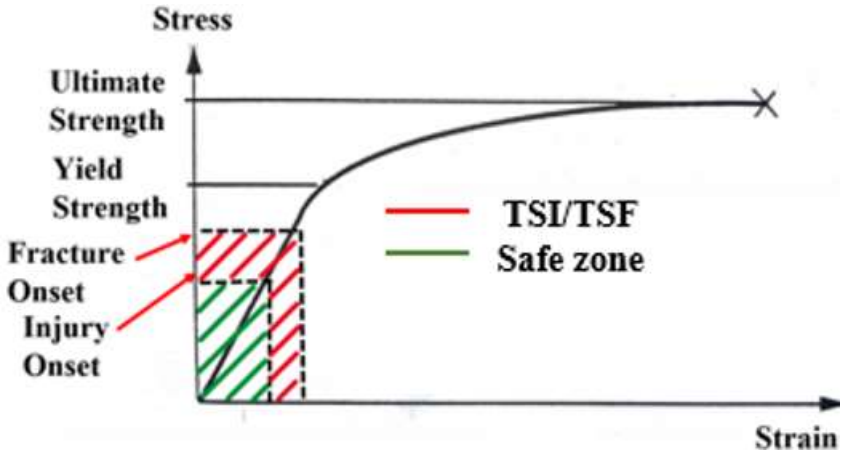

Figure 4-2. Measurements of Strength from the Stress-Strain Curve to Illustrate a Safe Zone for Individuals to Load the Injured Site Below the Injury Onset Threshold to Prevent Further Bone Damage.
The red region indicates the stress/strain when under repetitive loading, the mechanical properties of bone will fatigue over time allowing for the injury onset to occur at a threshold below the yield point. The green region indicates the stress/strain load an individual can operate at during the recovery period to help promote bone remodeling without further inducing bone damage. Modified with permission. Turner, C. H., & Burr, D. B. (1993). Basic biomechanical measurements of bone: a tutorial. Bone, 14(4), 595-608. doi:10.1016/8756-3282(93)90081-k [3].

remainder of the femur was then stripped of all tissue and potted in a cylindrical custom-made fixture mold to a depth of 2.5in where bismuth metal was poured into the mold. This process encased the remainder of the femur in a cylindrical metal case to interface with a cylindrical mating fixture within the robotic testing platform. An incision was made into the posterior aspect of the leg to expose the Achilles tendon and remove any muscular tissue attached to the tendon.

Loading Achilles Tendon

A predefined dead weight (50lbs) was used to provide a tensile load to the Achilles tendon during testing. This dead weight was roughly twenty-five percent of the applied load. Fixture construction provided a means to load the Achilles tendon in tension near physiological orientation. A Klein Tool wire pulling grip (KPS075 3/4in – 1in, Klein Tools, Lincolnshire, IL) was used to effectively grab onto and place the Achilles tendon in tension during testing without tearing the tissue.

Mounting Plate Fixture

A predefined dead weight (50lbs) was used to provide a tensile load to the Achilles tendon during testing. This dead weight was roughly twenty-five percent of the applied load. Fixture construction provided a means to load the Achilles tendon in tension near physiological orientation. A Klein Tool wire pulling grip (KPS075 3/4in – 1in, Klein Tools, Lincolnshire, IL) was used to effectively grab onto and place the Achilles tendon in tension during testing without tearing the tissue.

Strain Gauge Attachment

Linear strain gauges (794 kHz, 120Ω, C4A-06-235SL-120-39P, Micro-Measurements, Wendel, NC) were attached, as detailed by Micro-Measurement application procedure, to the anterior-medial tibia along the flat surface of the tibia bone. The strain gauges were attached at the distal tibia, 5cm above the medial malleoli, and the midpoint of the length of the tibia (Midshaft) for each specimen (**Figure 4-3**). These attachment sites were chosen based on the most common sites for tibial stress fractures [41,42,62,68,69]. Strain gauge wires were connected to a NI 9235 (8-Ch 24-Bit 120Ω, Quarter Bridge Analog Input, National Instruments, Austin, TX) attached to a cDAQ chassis module (cDAQ 9171, National Instruments, Austin, TX) connected to a desktop computer running LabView (LabView 2021, National Instruments, Austin, TX) to collect raw strain data. Equipment specifications are listed in **Appendix A** (**Table A-1**).

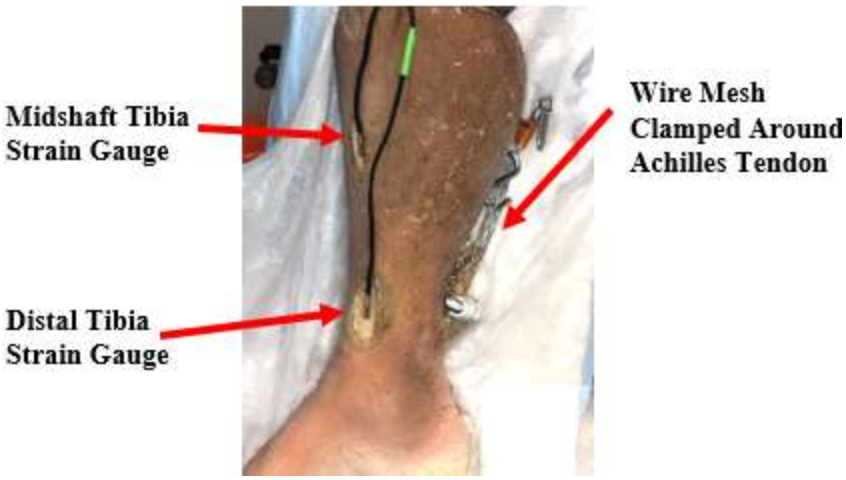

Figure 4-3. Strain Gauge Attachment of S1 at the Distal and Midshaft Attachment Sites with Wire Mesh to Grab the Achilles Tendon.

Orthosis Conditions

Two brace conditions were tested for this study: DAO (**Figure 4-4A**) and a standard of care walking boot (Össur FormFit Walker Air; **Figure 4-4B)**. The shoe used for the DAO condition (model 501, New Balance, Boston, MA) was modified with a metal stirrup embedded in the sole of the shoe to attach the upper orthosis components. In a previous study with the DAO, a targeted offloading of at least 10% of the participants body weight was recommended by orthotists regarding the level of offloading necessary to achieve pain reduction [13]. For testing purposes, the DAO was activated to offloaded 10% of the target load.

Experimental Protocol

Prior to inserting the specimen into the robotic testing platform, the specimen was wrapped in Press'n Seal plastic wrap (Glad, Oakland, CA) to help prevent fluids from escaping the specimen and contaminating to the DAO and walking boot. The specimen was then fitted with the selected brace condition and inserted into the robotic testing platform. For the DAO condition, Dycem Non-slip material (Dycem, Warwick, RI) was wrapped around the specimen to increase the coefficient of friction and allow the DAO to effectively grab onto the leg when pressurized to offload the leg. Wireless vertical force insoles (100Hz loadsol, Novel Electronics, St. Paul, MN) were inserted in the testing shoe to collect vertical force time-series data during testing. **Figure 4-5** shows the entire testing assembly and axis orientation. The specimen was mounted within the testing platform with the cylindrical portion of the femur potted in the bismuth metal alloy fixated into the custom cylindrical fixture mate. The base of the specimen foot was mounted on a rectangular base plate. The robot testing platform was in a neutral state when the specimen foot was in contact with the ground and the actuator was positioned so there was a vertical force reading of $-2N \leq F_z \leq 2N$ from the load cell with the weight of the leg resting on the force insoles (**Figure 4-6**). After the specimen was inserted into the robotic testing platform, the force insoles were calibrated using the manufacturer procedure before testing each brace condition. Each strain gauge was calibrated prior to running each testing condition. For the DAO condition, static offloading (10% applied load) was determined while in a loaded state by taking the percent difference of the insole force reading before and after pressurizing the pneumatic cylinders. While the robot actuator was in a neutral state a 50lbs (222.5N) dead weight was attached to a cable hooked to the wire mesh grip of the Achilles tendon to place the Achilles tendon in tension, pulling on the calcaneus allowing the arch of the foot to form. The robotic actuator applied a uniaxial load at 3.2mmps until a 900N load limit was reached for 5 dynamic cycles in both the DAO and walking boot conditions. Prior to dynamic cyclic testing, a static validation test was performed to validate the strain reduction between the DAO and walking boot and used to determine if the static strain magnitudes and strain rates were comparable to the dynamic testing conditions (**Figure C-3** and **Figure C-4**).

Strain at the distal and midshaft tibia along with insole vertical force-time series data were captured during each testing condition and processed within MATLAB

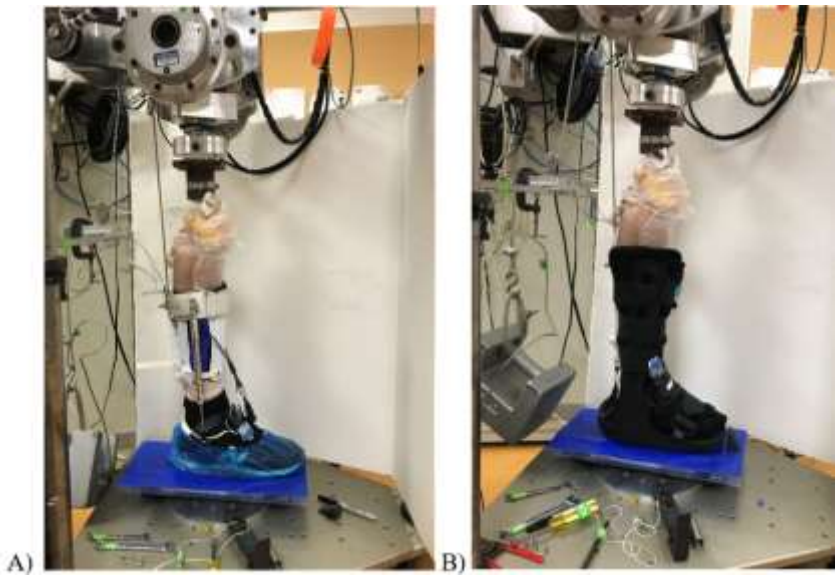

Figure 4-4. Cadaver Specimen (S1) Positioned in Robotic Testing Platform for Bracing Conditions.
DAO: Dynamic Ankle Orthosis. A) DAO and B) Walking Boot.

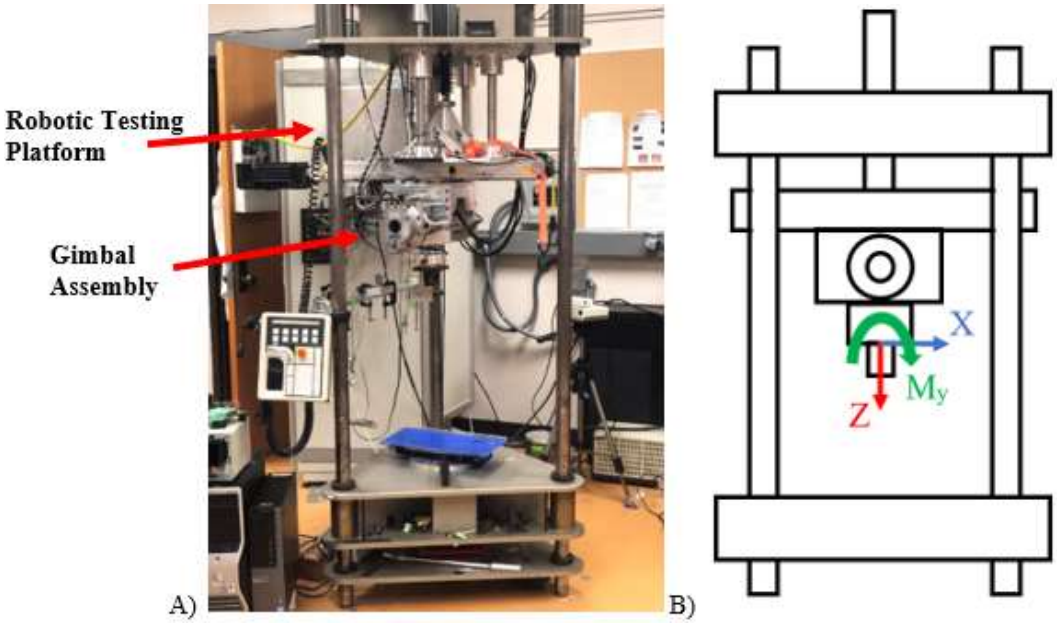

Figure 4-5. Robotic Testing Platform.
A) Image of the Robotic Testing Platform and B) Sketch of Testing Platform with Axis Orientation. The x-axis was along the anterior-posterior direction of the cadaver specimen. The y-axis was the medial-lateral axis of the cadaver specimen. The z-axis was along the longitudinal axis of the cadaver specimen.

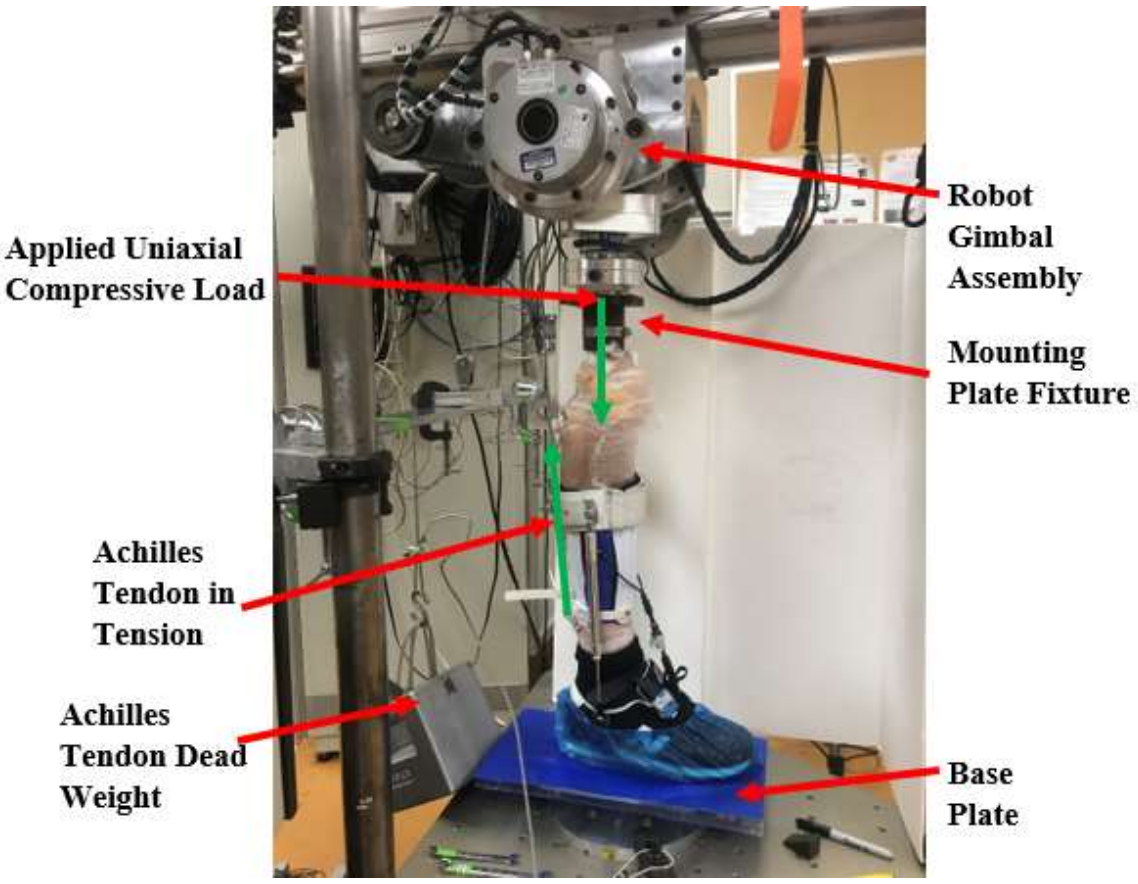

Figure 4-6. Test Setup of DAO Brace Condition.
DAO: Dynamic Ankle Orthosis

(MathWorks, Natick, MA). Raw strain and insole vertical force data were filtered using a low-pass Butterworth filter with a cutoff frequency of 5Hz and 8Hz, respectively, along with a moving average to help smooth the strain – time curve and force – time curve. Peak strain and vertical force values were determined from each testing condition along with the average strain rate and average vertical insole loading rate. Average strain/loading rate was determined by taking the change in strain/force divided by the change in time between 20 – 80% of the peak value. Pearson correlation was used to determine the relationship between strain and vertical insole reaction force measurements The percent offloading provided by the DAO compared to the walking boot was determined by taking the difference between the peak force in the DAO, $Force_{DAO,}$ and the peak force in the waking boot, $Force_{WB}$, divided by the peak force in the walking boot (**Equation 3-5**). Additional images about the experimental protocol and preliminary testing are listed in **Appendix B** (**Figure B-6** through **Figure B-8**).

Statistical Analyses

A Shapiro-Wilk test was used to assess normality of the data per condition for each dependent variable. A paired t-test with significance set at $p < 0.05$ was used to determine brace effect for all dependent variables that passed normality. Cohen's *d* effect size was determined to assess the effect size for differences between dependent variables (i.e., small: $d < 0.2$, medium: $0.2 \leq d < 0.8$, large: $d \geq 0.8$).

Results

Table 4-1 shows how the peak strain magnitude compared between the DAO and walking boot for each specimen (**Table 4-1**). The DAO had an effect on the peak strain and average strain rate compared to the walking boot (**Table 4-2).** A significant reduction in peak strain at the distal tibia occurred in the DAO (23.31%) relative to the walking boot (**Figure 4-7**). A similar reduction in the peak strain occurred at the midshaft tibia location of the DAO condition (33.54%) relative to the walking boot, however there was not a significant difference. Even though there was a large reduction in the average strain rate while wearing the DAO compared to the walking boot (**Figure 4-8**), there was not a significant difference at the distal tibia (39.28%) but there was a significant difference at the midshaft tibia (45.0%). An example of the strain-time graph can be seen for the DAO and walking boot in **Appendix B** (**Figure B-9** and **Figure B-10**). **Table 4-3** showed the vertical reaction force data between the DAO and walking boot. The DAO reduced the peak vertical force by 20.29% compared to the walking boot under dynamic loading conditions, but the differences were not significant (**Figure 4-9**). The average insole loading rate did show a significant reduction when wearing the DAO (**Figure 4-10**).

Pearson correlation between strain and vertical force was obtained by normalizing the strain and vertical force data to 500 points to represent the dynamic loading conditions (**Table 4-4**). Plotting the compressive strain against the insole vertical reaction force for each specimen (**Figures 4-11** through **4-14**) showed moderate to strong negative

Table 4-1. Peak Strain (με) Data for Individual Specimens Under Uniaxial Loading.

		Distal Tibia		Midshaft Tibia	
Specimen	**Sex**	**DAO**	**Walking Boot**	**DAO**	**Walking Boot**
S1	Male	230 ± 4	398 ± 3	241 ± 1	336 ± 3
S2	Female	753 ± 9	826 ± 13	473 ± 10	795 ± 4
S3	Male	94 ± 1	180 ± 2	160 ± 5	184 ± 1

Mean ± Standard Deviation. DAO: Dynamic Ankle Orthosis.

Table 4-2. Peak Strain and Average Strain Rate for the Distal and Midshaft Tibia in Each Brace Condition During Uniaxial Loading.

Variables	Gauge Location	DAO	Walking Boot	*P* Value	Effect Size (*d*)	Percent Offloading
Peak Tibia Strain (με)[a]	Distal	359 ± 348*	468 ± 329	0.034	2.11	23.31
	Midshaft	291 ± 162	438 ± 318	0.122	0.94	33.54
Average Strain Rate (με/s)[a]	Distal	53 ± 56	88 ± 45	0.099	1.09	39.29
	Midshaft	52 ± 23*	94 ± 42	0.032	2.17	45.00

Mean ± Standard Deviation. [a] Brace effect ($p < 0.05$). DAO: Dynamic Ankle Orthosis.
* Denotes significant difference from walking boot. Effect size: small effect = $d < 0.2$, medium effect = $0.2 \leq d < 0.8$, large effect = $d \geq 0.8$.

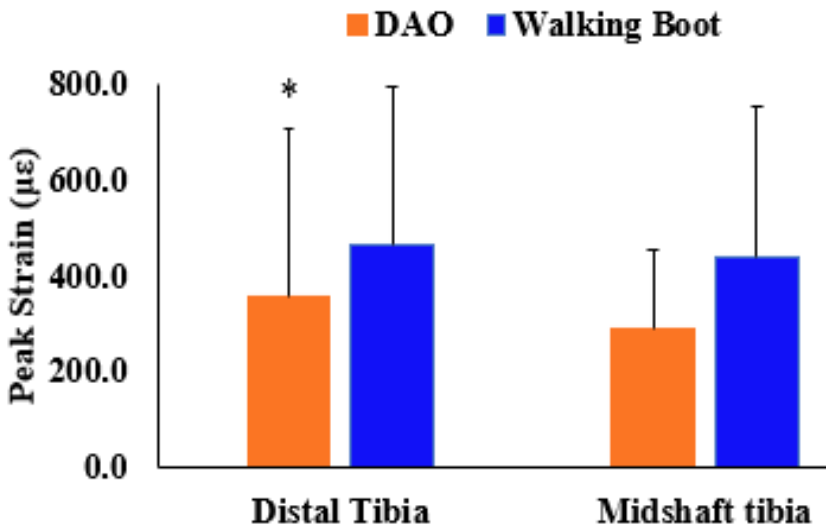

Figure 4-7. Peak Strain (με) During Uniaxial Loading Between Brace Conditions: DAO and Walking Boot; and Strain Gauge Locations: Distal Tibia and Midshaft Tibia.
DAO: Dynamic Ankle Orthosis. * Denotes significant difference from walking boot.

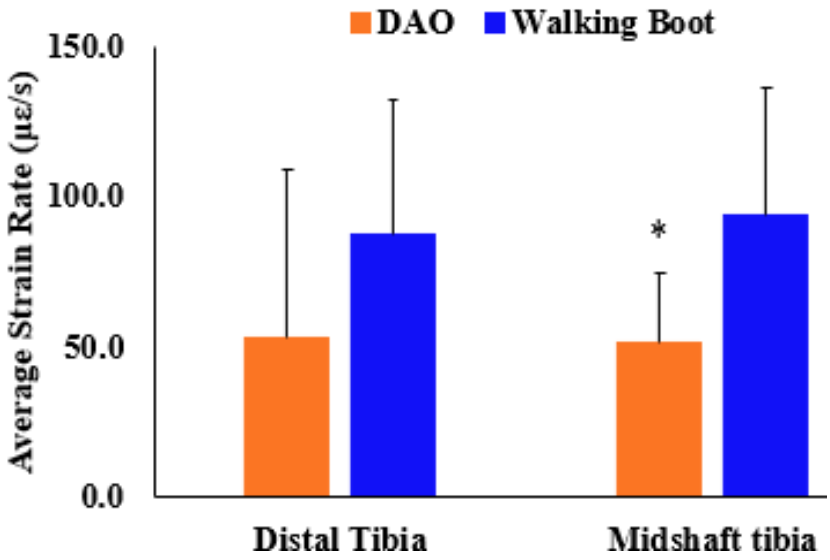

Figure 4-8. Average Strain Rate (με/s) During Dynamic Uniaxial Loading Between Brace Conditions: DAO and Walking Boot; and Strain Gauge Locations: Distal Tibia and Midshaft Tibia.
DAO: Dynamic Ankle Orthosis. * Denotes significant difference from walking boot.

Table 4-3. Insole Peak Vertical Force and Average Loading Rate in Each Brace Condition During Uniaxial Loading.

Variable	DAO	Walking Boot	*P* value	Effect size (*d*)	Percent Offloading
Peak Vertical Force (N)	656 ± 47	827 ± 134	0.078	1.29	20.65
Average Loading Rate (N/s)[a]	137 ± 35*	223 ± 32	0.033	2.12	38.56

Mean ± Standard Deviation. DAO: Dynamic Ankle Orthosis. [a] Brace effect ($p < 0.05$). * Denotes significant difference from walking boot. Effect size: small effect = $d < 0.2$, medium effect = $0.2 \leq d < 0.8$, large effect = $d \geq 0.8$.

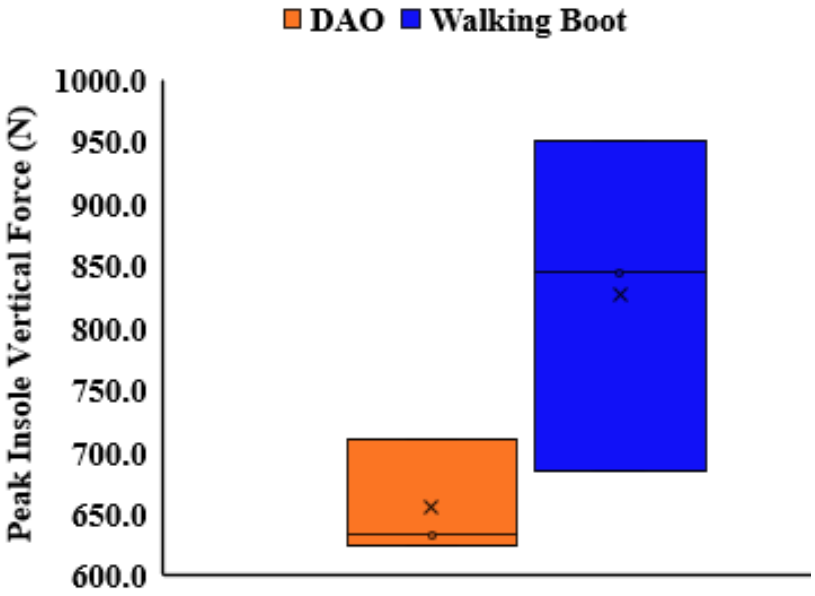

Figure 4-9. Peak Insole Vertical Force (N) During Uniaxial Loading Between Brace Conditions: DAO and Walking Boot.
DAO: Dynamic Ankle Orthosis. * Denotes significant difference from walking boot.

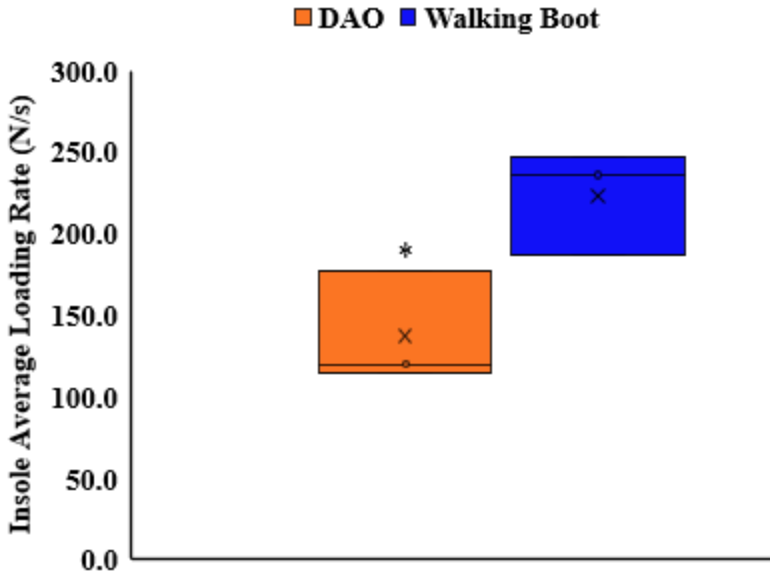

Figure 4-10. Insole Average Loading Rate (N/s) During Uniaxial Loading Between Brace Conditions: DAO and Walking Boot.
DAO: Dynamic Ankle Orthosis. * Denotes significant difference from walking boot.

Table 4-4. Distal Tibia Pearson Correlation for Strain Data Compared to Vertical Reaction Force Data.

Specimen	Gauge Location	R_{DAO}	*P* Value	R_{WB}	*P* Value
S1	Distal	-0.69	<0.001	-0.87	<0.001
	Midshaft	-0.66	<0.001	-0.86	<0.001
S2	Distal	-0.68	<0.001	-0.85	<0.001
	Midshaft	-0.64	<0.001	-0.84	<0.001
S3	Distal	-0.80	<0.001	-0.84	<0.001
	Midshaft	-0.79	<0.001	-0.81	<0.001
Average	Distal	-0.72	<0.001	-0.84	<0.001
	Midshaft	-0.71	<0.001	-0.81	<0.001

DAO: Dynamic Ankle Orthosis. WB: Walking Boot. Data was normalized to 500 data points between the start and stop of data collection. $p < 0.05$; weak relationship = $0.3 < r < 0.5$, moderate relationship = $0.5 < r < 0.7$, strong relationship = $r > 0.7$.

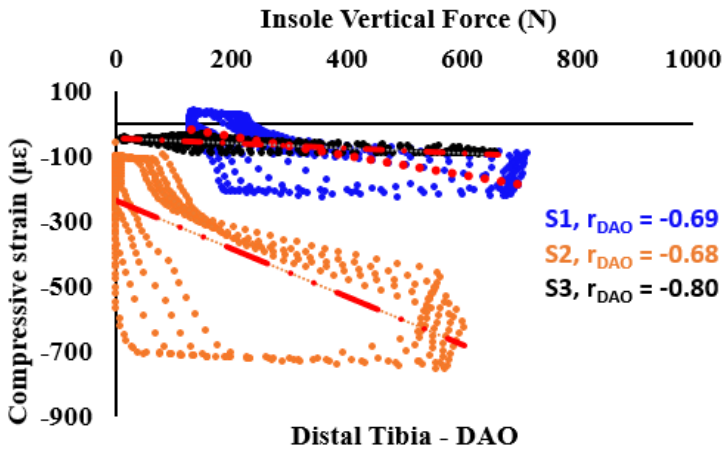

Figure 4-11. DAO Pearson Correlation (r) for Peak Compressive Strain (με) Compared to Vertical Reaction Force (N) for Five Loading Cycles at the Distal Tibia.
DAO: Dynamic Ankle Orthosis.

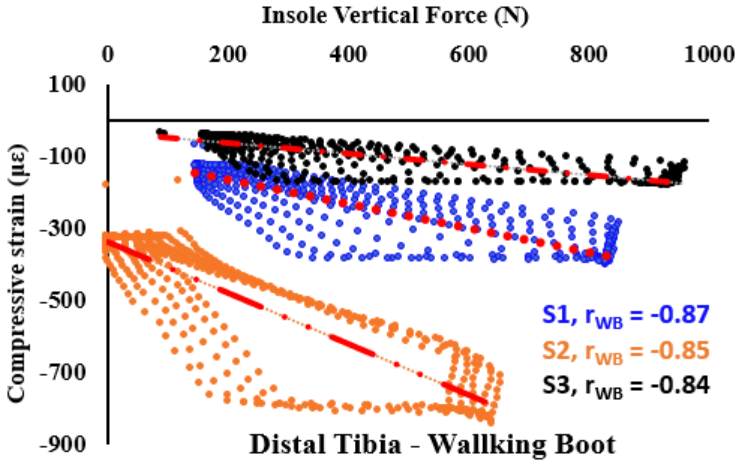

Figure 4-12. Walking Boot Pearson Correlation (r) for Peak Compressive Strain (με) Compared to Vertical Reaction Force (N) for Five Loading Cycles at the Distal Tibia.
WB: Walking Boot.

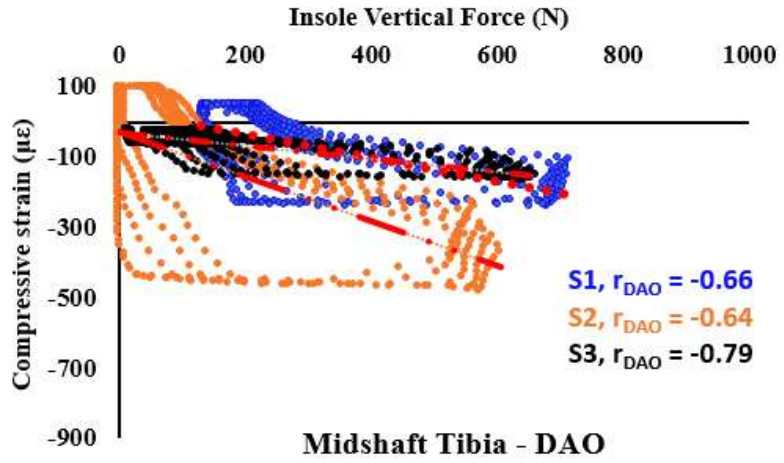

Figure 4-13. DAO Pearson Correlation (r) for Peak Compressive Strain (με) Compared to Vertical Reaction Force (N) for Five Loading Cycles at the Midshaft Tibia.
DAO: Dynamic Ankle Orthosis.

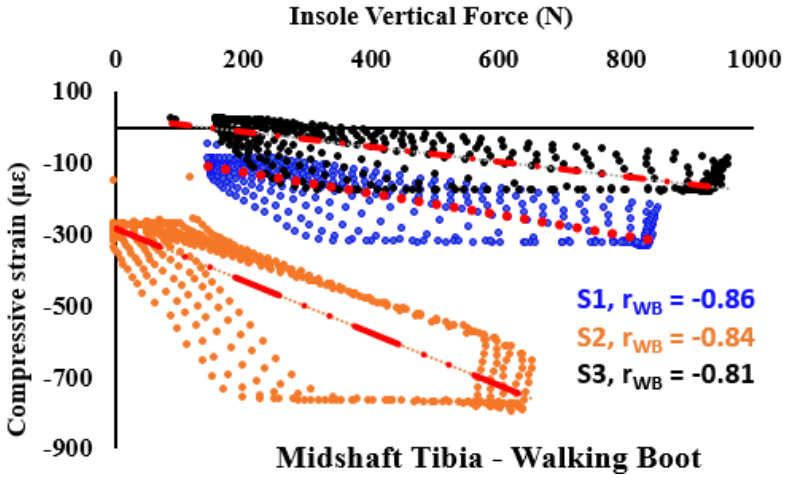

Figure 4-14. Walking Boot Pearson Correlation (r) for Peak Compressive Strain (με) Compared to Vertical Reaction Force (N) for Five Loading Cycles at the Midshaft Tibia.
WB: Walking Boot.

linear correlations. Specimen two (female) showed the weakest correlation for both the distal and midshaft tibia while wearing the DAO and only the distal tibia in the walking boot due to having the greatest dispersion of data points from the from the linear fit during loading and unloading cycles.

Discussion

The purpose of this study was to determine the offloading effects of the DAO on tibial bone strain and vertical reaction force compared to a standard of care walking boot in a human cadaver model. The results partially support an apparent brace effect. Our results partially support our first hypothesis that the DAO would reduce the strain magnitude and strain rate compared to the walking boot. Under dynamic loading conditions, the DAO was able to reduce the peak strain, compared to the walking boot, at the distal tibia (23.31%, $d = 2.12$, $p = 0.034$) however, no significant reduction was observed at the midshaft tibia (33.54%, $d = 0.94$, $p = 0.122$) even though there was a greater reduction in the strain magnitude when wearing the DAO compared to the walking boot. The lack of significance at the midshaft of the tibia could be attributed to a couple of different factors. First is our small sample size. Because of this, it is more relevant to pay attention to the effect size rather than the p – value for our statistical results. Increasing our sample size will likely provide a significant difference in the peak strain at the midshaft tibia. Second, the large standard deviation between each specimen.

The peak strain differed greatly between specimens (**Table 4-2**). Specimen two experienced much larger strain deformation compared to the other two specimens. It is possible that this is because specimen two was a 55yr old female. At this age, women often have mild to severe osteoporosis, leading to decreased bone quality affecting the amount of deformation the tibia would experience. When wearing the DAO, the peak strain differed between the distal and midshaft tibia strain gauge locations which makes sense considering the cross-sectional area of the tibia increases you move from the distal to a more proximal area of the tibia. When wearing the walking boot, the peak strain at the distal and midshaft tibia were similar during testing. Strongly suggesting that the rigid design of the walking boot constrained the tibia, increasing the load throughout the tibia length. Compared to the peak strain, the opposite affect happened where the strain rate was significantly reduced at the midshaft tibia (45%, $d = 2.17$, $p = 0.032$) but not at the distal tibia (39.29%, $d = 1.09$, $p = 0.099$) compared to the walking boot. The strain rate measurements observed in the current study do fall well short of those observed during *in vivo* studies [60,62,70,71]. This was primarily due to the robotic actuator moving at 50% of its capacity, however this does provide evidence of the ability of the DAO to dampen the applied load.

Our second hypothesis that there would be an equivalent reduction in strain along with the vertical reaction force was partially supported. With the initial target offload of 10% body weight from the DAO, there was a 20.7% reduction in the peak vertical reaction force along with a 23.3% reduction in the peak strain at the distal tibia in the DAO compared to the walking boot. The amount of externally applied offload provided

about twice as much internal offloading. Showing potential to gain an understanding of the percent reduction in strain by monitoring the amount of offloading from the VRF.

Lastly, our third hypothesis was supported. There were moderate to strong Pearson correlations when comparing the strain and VRF for the DAO and Walking Boot (**Table 4-4**) for both the distal and midshaft tibia. Looking at **Figures 4-11** to **4-14**, for each specimen, the DAO reduced the starting and end strain magnitudes compared to when wearing the walking boot. The walking boot did provide a stronger negative linear correlation compared to the DAO, but the rigid design of the boot to constrain the tibia increased the strain magnitude experienced during testing [60,62,71-73]. S2 showed a greater variation in strain measurements from the linear fit compared to S1 and S2. Again, this could be due to gender differences between specimens and the quality of bone for S2.

Even though we were unable to replicate the loading rate from Study 1 (**Chapter 3**), The strain measurements we observed during this study fell within the lower spectrum of what previous researchers have observed during *in vivo* walking measurements. The recorded strain measurements in our study were between 290 - 470με of compression whereas *in vivo* studies demonstrated compressive strain measurements between 290 - 700με during walking (**Figure 4-15**). Even though the strain values observed are similar to what has been observed in previous studies, these values may have been limited by the rate at which the robotic testing platform was able to move. The movement speed of the actuator was tested at 50% of the max capacity (3.2mm/s) to prevent any damage from occurring to the robotic testing platform, load cell, and cadaveric tissue. Based on current literature, increased strain rates of the tibia have been associated with more physically demanding activities [60,71].

To the best of our knowledge, this study is the first to examine the strain experienced at common tibial stress fracture locations while wearing a walking boot. A cadaveric model provided a practical means for observing the desired parameters. Other studies that examine the strain experienced by the tibia consist of *in vivo* studies. Today, it is extremely difficult to perform *in vivo* strain measurements due to Institutional Review Board limitations. Our study addresses the mechanical loading environment of the tibia while wearing a brace to provide helpful information to understand how constraining the tibia affects the loading environment. Milgrom et al., 2000, analyzed stress fracture incidence rates and the midtibia strain measurements from infantry recruits *in vivo* during basic training. They observed a maximum of 561με in recruits walking at 5khm/hr. In a separate study, Milgrom et al., 2002 observed between 415με and 571με in participants for barefoot treadmill walking and treadmill walking in running shoes, respectively. Edwards et al., 2009 found moderate to strong, positive, linear correlations for calculating bone strain from impact force at the distal tibia during cadaveric impact activity, showing an increase in bone strain as the impact force increased. Along with our results, there is potential to gain an understanding of the internal loading environment of the tibia outside of the laboratory or within a clinical setting by utilizing instrumented force insoles.

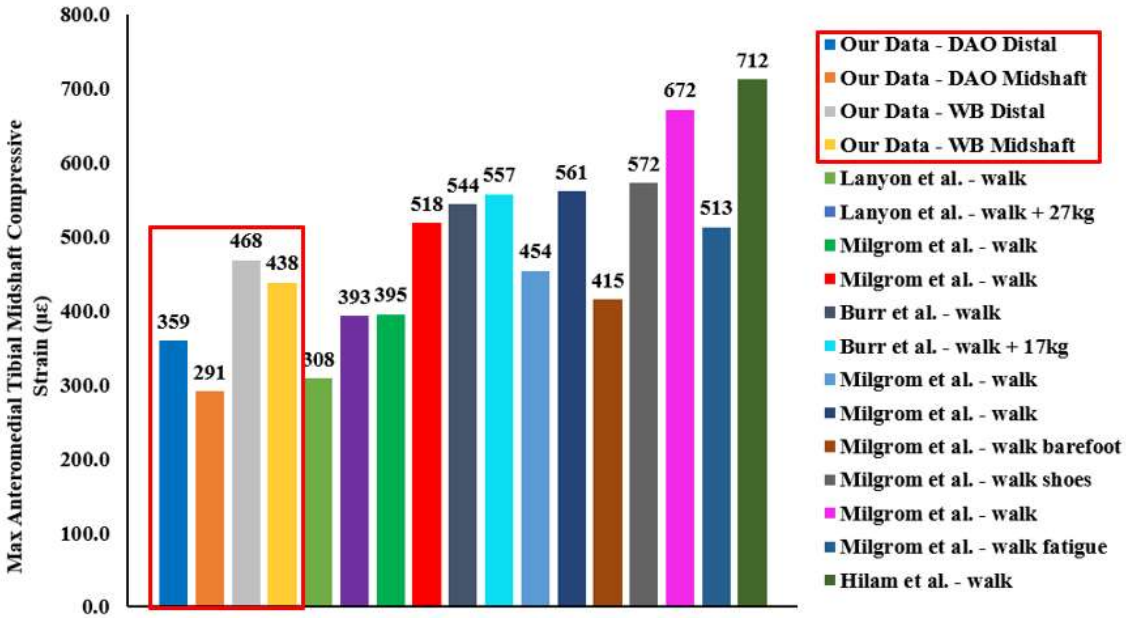

Figure 4-15. Peak Strain Magnitude (με) from the Current Study Compared to Previous Literature.

DAO: Dynamic Ankle Orthosis. Source data: Hadid, A., Epstein, Y., Shabshin, N., & Gefen, A. (2018). Biomechanical Model for Stress Fracture-related Factors in Athletes and Soldiers. Med Sci Sports Exerc, 50(9), 1827-1836. https://doi:10.1249/MSS.0000000000001628 [72]

The small sample size of this study (n=3) limits the ability to generalize the results to a larger population size. It is important to note that this study only observed the compressive uniaxial load along the longitudinal axis of the tibia at two specific locations, the midshaft and distal aspect of the medial tibia. Specimen anatomy was an extraneous variable that can affect the average strain gauge measurements. It was apparent that the strain measurements at the distal and midshaft tibia differed greatly between each specimen. This can be attributed to the bone quality and its resistance to the applied load. For the individual female specimen (S2) there was noticeable knee valgus that prevented the leg from being perfectly aligned to the vertical axis of the robotic testing platform and the applied load and could influence the strain output. Post-menopausal osteoporosis likely affected the bone quality of the tibia leaving the bone more susceptible to deformation. Strain gauge placement is a factor that could affect the strain output. Strain gauges at the midshaft and distal tibia were applied by hand using the Micro-measurements application procedure. Human error could prevent the strain gauges from being perfectly aligned with the longitudinal axis and the direction of grain of the tibia. The adhesive attaching the strain gauge to the tibia could affect strain measurements by the amount of deformation the glue allows the gauge to undergo in response to the deformation of the bone.

The loading scenario used in this study was primarily used to validate the offloading capabilities of the DAO and only utilized a uniaxial load rather than a loading scenario that closely mimics the stance phase of gait. Strain measurements may differ under more physiological loading conditions. Additionally, we only targeted an applied load of 900N due to the limitations of the loadcell uniaxial load limits. Studies have shown that the tibia experiences much greater mechanical loads (25, Ground reaction force metrics; Scott et al., 1989, Internal forces at chronic running injury sites) primarily due to contractive muscle contribution. A testing platform that could apply enough of a force to closely replicate the estimated tibial load and loading rates could produce strain measurements that are more representative of that which the tibia would experience under a physiologic loading condition. While we only applied a uniaxial load, a future direction would be for us to maneuver the cadaveric leg through flexion and extension similar to that of stance phase of walking to obtain more physiological strain measurements and monitoring how the tibial bone strain changes throughout the stance phase, using a rosette strain gauge to also capture tensile and shear strain. Shear strain has shown to be greater than compressive/tensile strain during exercise activities [62,64,69,73]. Turner and Burr (1993) mentioned that materials, when experiencing a compressive load, will likely fail due to shear strain because most material are not as strong under shear as they are under compression and these compressive loads create shear stress at 45° angle. When determining shear fatigue failure, Turner et al., found that the fatigue life of a femoral cortical bone can be as much as 3 orders of magnitude shorter in shear compared to compression [74]

Conclusion

In conclusion, the results obtained from this study are relevant for both researchers and clinicians in understanding the loading environment of the tibia in different brace conditions. The DAO provided a distractive force to offload the lower limb, primarily at the distal tibia, during uniaxial loading in addition to reducing the insole vertical reaction force. Percent reduction in the vertical reaction force measurements compared to the distal strain measurements were close but differed further away from the ankle joint. The moderate to strong correlations between bone strain and insole vertical reaction force measurements suggests that wearable technology has potential to be used as a surrogate to understand the bone strain of the distal and midshaft tibia as a non-invasive means of measurement. The information gathered from the walking boot is helpful to determine the offloading capabilities of a walking boot to reduce the mechanical loads of the tibia. Using the DAO, tibial stress fracture patients could potentially offload the injured limb to reduce the axial strain and strain rate to a level that could allow the bone to heal at a more efficient rate by providing minimal mechanical stimulation, potentially shortening the recovery period and a quicker return to sport for athletes.

CHAPTER 5. DISCUSSION: RELATING OUTCOMES BETWEEN STUDY 1 AND STUDY 2

The purpose of this research was to determine the effects of an alternative orthosis brace that provides a distractive force to the tibia to assess its feasibility for use on treating tibial stress fractures compared to a standard of care walking boot. Two studies were performed: 1) *in vivo* study in a gait lab with healthy individuals with external measures to quantify tibial bone loading and 2) in vitro study on a human cadaveric model with direct measures of tibial bone strain.

The combination of the reduced moment arm and reduced vertical force component from the distractive force of the DAO reduced the mechanical loading environment of the tibia while also retaining natural ankle mobility. For study 1, the reduced moment arm of the DAO (between the vertical force and ankle joint) translated to less plantarflexor muscle force needed to overcome the external ankle moment compared to the longer moment arm of the walking boot due to its rigid design. This design difference helps to reduce the force production of the Achilles tendon and overall tibial compressive force. Even though the insole vertical reaction force, VRF_z, was similar between the DAO and walking boot during treadmill walking, it is important to note that this is only at the instance in time of peak plantarflexor moment. At a point in time during the first half of stance phase, the vertical force is likely to be different. Further analysis of the first fifty percent of stance phase showed a large reduction in the peak insole vertical force ($d = 0.73$, $p < 0.05$; **Figure C-1**) between the DAO (0.85 BW) and the walking boot (0.92 BW).

The results from study 2 demonstrate the ability of the DAO to reduce the vertical force component. Even though we did not replicate a physiological loading environment, we were able to replicate similar strain measurements from previous *in vivo* studies. The DAO showed the ability to significantly reduce the strain magnitude and strain rate at the distal and midshaft tibia, respectively. The DAO allows for a patient to retain the mobility of their ankle during the rehabilitation period and potentially limit the amount of muscle atrophy that occurs. The reduced muscle atrophy could shorten the additional recovery time an individual would need to recondition the muscle tissue prior to returning to their sport. It might also be worth noting that the reduced required force production at the Achilles tendon could be beneficial for individuals who have sustained an Achilles injury or from overuse injury. The DAO could allow individuals to stay active without increasing stress on the Achilles tendon, especially since there is no current gold standard of treatment for Achilles injuries such as Achilles tendonitis [50].

CHAPTER 6. FUTURE WORK

Considerations for Future Research

Previous validation and gait analysis of the DAO [15-17], established a strong foundation that the two recent research studies were able to build upon. The DAO has undergone several design modifications since the device was first developed for performance, comfort, and simplicity improvements to help make the device more marketable. However, further modifications can be incorporated to help make the device more user friendly. An off-the-shelf bike pump was necessary to pressurize the pneumatic cylinders of the DAO. While this was feasible for the current studies, this would not be ideal for an individual with a TSF who would be required to wear the device for several weeks. An easily accessible inflatable pump or gas springs with a set force output would need to be installed into the DAO for convenience.

The rocker design and rigidity of the walking boot to constrain the ankle joint created a greater moment arm during walking, leading to a greater external ankle moment and subsequently a greater Achilles load. Even though the DAO allowed for increased ankle mobility in the sagittal plane, the Achilles tendon force was reduced. Initially, without data, it might predict that the near normal activity of the plantarflexor muscles wearing the DAO would create more force production. However, this was not the case. The increased ankle mobility of the DAO provided participants with the ability to raise their heel and pivot at the metatarsal joint, reducing the moment arm, reducing the external ankle moment and the Achilles Load. The use of electromyography sensors could be utilized in a pilot study with a similar methodology to the treadmill walking study. Attaching EMG sensors to the plantarflexor muscles under a control, DAO, and walking boot condition and assessing the EMG activity during stance phase, relative to the control condition can help provide further information about the amount of muscle involvement in the different brace conditions.

The findings from these two studies have relevance for both researchers and clinicians in understanding the loading environment of the tibia in different brace conditions. In this study, a target offload for the DAO of 10% body weight was recommended by a group of orthotists and found to reduce the tibial compressive force and Achilles tendon force by applying a distractive force across the lower leg and ankle joint. The next phase of the research should investigate the clinical benefits of extended brace wear during the rehabilitation phase on TSF patients. Our results indicated that the 10% offloading was sufficient to provide a significant difference between brace conditions, however clinical relevance is still warranted for comfort and healing. Further testing would be needed to investigate whether increasing the amount of offloading would provide greater reductions in the tibial compressive force and Achilles tendon force without compromising patient comfort.

Previous clinical assessment of the DAO while performing function activities for patients suffering from chronic ankle diseases such as osteoarthritis, post-traumatic ankle

osteoarthritis, posterior tibialis tendon dysfunction, and chronic postoperative pain showed improvement of pain symptoms [17]. Military personnel and high school runners are two groups at risk of developing tibial stress fractures [4,75]. To further understand the effect the DAO has on the mechanical loading environment of the tibia, future work should include outfitting tibial stress fracture patients with the DAO or walking boot and monitoring the rate of bone union and the amount of muscle atrophy that occurs during the rehabilitation period. It may also be warranted to perform an *in vivo* pilot study by connecting strain gauges to a participant's tibia at common stress fracture locations to directly measure the strain while wearing the DAO during various physical exercises to validate the concept from study 2 that the DAO does provide a reduction in strain.

Conclusions

This body of work adds to the existing evidence to use the DAO over a traditional walking for treating TFS. The DAO provided significant reduction of the tibial compressive force and Achilles Tendon force at peak plantarflexor moment during treadmill walking while maintaining sagittal ankle mobility compared to a standard of care walking boot. Additionally, aspects of this work provided further evidence that the offloading features of the DAO directly reduced bone strain under simulated stance phase loading conditions. This could aid the bone healing process during the recovery phase of a tibial stress fracture and improve clinical outcomes. Further validation of the DAO to provide sufficient offloading during the recovery period, can be used to adapt the current treatment method for TSF and help patients return to their sport.

LIST OF REFERENCES

1. Matheson, G. O., Clement, D. B., McKenzie, D. C., Taunton, J. E., Lloyd-Smith, D. R., & MacIntyre, J. G. (1987). Stress fractures in athletes. A study of 320 cases. Am J Sports Med, 15(1), 46-58. doi:10.1177/036354658701500107.
2. Pattin, C. A., Caler, W. E., & Carter, D. R. (1996). Cyclic mechanical property degradation during fatigue loading of cortical bone. J Biomech, 29(1), 69-79. doi:10.1016/0021-9290(94)00156-1
3. Turner, C. H., & Burr, D. B. (1993). Basic biomechanical measurements of bone: a tutorial. Bone, 14(4), 595-608. doi:10.1016/8756-3282(93)90081-k
4. Wood, A. M., Hales, R., Keenan, A., Moss, A., Chapman, M., Davey, T., & Nelstrop, A. (2014). Incidence and Time to Return to Training for Stress Fractures during Military Basic Training. J Sports Med (Hindawi Publ Corp), 2014, 282980. doi:10.1155/2014/282980
5. Bennell, K. L., Malcolm, S. A., Thomas, S. A., Reid, S. J., Brukner, P. D., Ebeling, P. R., & Wark, J. D. (1996). Risk factors for stress fractures in track and field athletes. A twelve-month prospective study. Am J Sports Med, 24(6), 810-818. doi:10.1177/036354659602400617.
6. Nikander, R., Kannus, P., Rantalainen, T., Uusi-Rasi, K., Heinonen, A., & Sievanen, H. (2010). Cross-sectional geometry of weight-bearing tibia in female athletes subjected to different exercise loadings. Osteoporos Int, 21(10), 1687-1694. doi:10.1007/s00198-009-1101-0
7. Wentz, L., Liu, P. Y., Haymes, E., & Ilich, J. Z. (2011). Females have a greater incidence of stress fractures than males in both military and athletic populations: a systemic review. Mil Med, 176(4), 420-430. doi:10.7205/milmed-d-10-00322
8. Dugan, S. A., & Weber, K. M. (2007). Stress fractures and rehabilitation. Phys Med Rehabil Clin N Am, 18(3), 401-416, viii. doi:10.1016/j.pmr.2007.04.003.
9. Liem, B. C., Truswell, H. J., & Harrast, M. A. (2013). Rehabilitation and return to running after lower limb stress fractures. Curr Sports Med Rep, 12(3), 200-207. doi:10.1249/JSR.0b013e3182913cbe
10. DiLiberto, F. E., Baumhauer, J. F., Wilding, G. E., & Nawoczenski, D. A. (2007). Alterations in plantar pressure with different walking boot designs. Foot Ankle Int, 28(1), 55-60. doi:10.3113/FAI.2007.0010
11. Baumhauer, J. F., Wervey, R., McWilliams, J., Harris, G. F., & Shereff, M. J. (1997). A comparison study of plantar foot pressure in a standardized shoe, total contact cast, and prefabricated pneumatic walking brace. Foot Ankle Int, 18(1), 26-33. doi:10.1177/107110079701800106
12. Lajevardi-Khosh, A., Bamberg, S., Rothberg, D., Kubiak, E., Petelenz, T., & Hitchcock, R. (2019). Center of pressure in a walking boot shifts posteriorly in patients following lower leg fracture. Gait Posture, 70, 218-221. doi:10.1016/j.gaitpost.2019.03.010
13. Patel, D. S., Roth, M., & Kapil, N. (2011). Stress fractures: diagnosis, treatment, and prevention. Am Fam Physician, 83(1), 39-46. Retrieved from https://www.ncbi.nlm.nih.gov/pubmed/21888126
14. Roberts, C. L., Meyering, C. D., & Zychowicz, M. E. (2014). Improving the

management of tibia stress fractures: a collaborative, outpatient clinic-based quality improvement project. Orthop Nurs, 33(2), 75-83; quiz 84-75. doi:10.1097/NOR.0000000000000032
15. Chung, C. L., DiAngelo, D.J. (2018). Design and validation testing of a dynamic ankle orthosis. MOJ App Bio Biomech. 2(3):210–217. doi:10.15406/mojabb.2018.02.00069.
16. Chung, C. L., DiAngelo, D. J., Powell, D. W., & Paquette, M. R. (2020). Biomechanical Comparison of a New Dynamic Ankle Orthosis to a Standard Ankle-Foot Orthosis During Walking. J Biomech Eng, 142(5). doi:10.1115/1.4045549.
17. Chung, C. L., Paquette, M. R., & DiAngelo, D. J. (2021). Impact of a dynamic ankle orthosis on acute pain and function in patients with mechanical foot and ankle pain. Clin Biomech (Bristol, Avon), 83, 105281. doi:10.1016/j.clinbiomech.2021.105281
18. Betts, J. G., Johnson, E., Wise, J. A., & Young, K. A. (2020). Planes of the Body. In Anatomy and Physiology: OpenStax. Retrieved from https://assets.openstax.org/oscms-prodcms/media/documents/AnatomyandPhysiology-OP.pdf
19. Venkadesan, M., Yawar, A., Eng, C.M., Dias, M.A., Singh, D.K., Tommasini, S.M., Haims, A.H., Bandi, M.M., & Mandre, S. (2020). Stiffness of the human foot and evolution of the transverse arch. Nature, 579,104. https://www.nature.com/articles/s41586-020-2053-y
20. Brockett, C. L., & Chapman, G. J. (2016). Biomechanics of the ankle. Orthop Trauma, 30(3), 232-238. doi:10.1016/j.mporth.2016.04.015
21. Hughes, J., & Jacobs, N. (1979). Normal human locomotion. Prosthet Orthot Int, 3(1), 4-12. doi:10.3109/03093647909164693
22. Neumann D. A. (2016). Kinesiology of the Musculoskeletal System: Foundations for Rehabilitation. Mosby, 3, 606. Retrieved from https://www.elsevier.com/books/kinesiology-of-the-musculoskeletal-system/neumann/978-0-323-28753-1 on November 1, 2022.
23. Flores, D.V., Gomez, C.M., Hernando, M.F., Davis, M.A., Pathria, M.N. (2019). Adult acquired flatfoot deformity: anatomy, biomechanics, staging, and imaging findings. RadioGraphics, 39, 1438. https://doi.org/10.1148/rg.2019190046
24. Pirker, W. & Katzenschlager, R. (2017). Gait disorders in adults and the elderly. The Central European Journal of Medicine, 129, 82. doi:10.1007/s00508-016-1096-4
25. Matijevich, E. S., Branscombe, L. M., Scott, L. R., & Zelik, K. E. (2019). Ground reaction force metrics are not strongly correlated with tibial bone load when running across speeds and slopes: Implications for science, sport and wearable tech. PLoS One, 14(1), e0210000. doi:10.1371/journal.pone.0210000
26. Meardon, S. A., Derrick, T. R., Willson, J. D., Baggaley, M., Steinbaker, C. R., Marshall, M., & Willy, R. W. (2021). Peak and Per-Step Tibial Bone Stress During Walking and Running in Female and Male Recreational Runners. Am J Sports Med, 49(8), 2227-2237. doi:10.1177/03635465211014854
27. Scott, S. H., & Winter, D. A. (1990). Internal forces of chronic running injury sites. Med Sci Sports Exerc, 22(3), 357-369. Retrieved from

https://pubmed.ncbi.nlm.nih.gov/2381304/
28. Matijevich, E. S., Scott, L. R., Volgyesi, P., Derry, K. H., & Zelik, K. E. (2020). Combining wearable sensor signals, machine learning and biomechanics to estimate tibial bone force and damage during running. Hum Mov Sci, 74, 102690. doi:10.1016/j.humov.2020.102690
29. Rodan, G.A. (2003). The development and function of the skeleton and bone metastases. Cancer, 97(3), 728. doi:10.1002/cncr.11147
30. Katsimbri, P. (2017). The biology of normal bone remodelling. Eur J Cancer Care (Engl), 26(6). doi:10.1111/ecc.12740.
31. Wolff, J. (1986). The law of bone remodelling. Springer Science & Business Media.
32. Burr, D. B., Milgrom, C., Boyd, R. D., Higgins, W. L., Robin, G., & Radin, E. L. (1990). Experimental stress fractures of the tibia. Biological and mechanical aetiology in rabbits. J Bone Joint Surg Br, 72(3), 370-375. doi:10.1302/0301-620X.72B3.2341429
33. Burr, D. B. (1997). Bone, exercise, and stress fractures. Exerc Sport Sci Rev, 25, 171-194. Retrieved from https://pubmed.ncbi.nlm.nih.gov/9213092/
34. Edwards, W. B., Ward, E. D., Meardon, S. A., & Derrick, T. R. (2009). The use of external transducers for estimating bone strain at the distal tibia during impact activity. J Biomech Eng, 131(5), 051009. doi:10.1115/1.3118762
35. Crincoli, M. G., & Trepman, E. (2001). Immobilization with removable walking brace for treatment of chronic foot and ankle pain. Foot Ankle Int, 22(9), 725-730. doi:10.1177/107110070102200907
36. Warden, S. J., Edwards, W. B., & Willy, R. W. (2021). Optimal Load for Managing Low-Risk Tibial and Metatarsal Bone Stress Injuries in Runners: The Science Behind the Clinical Reasoning. J Orthop Sports Phys Ther, 51(7), 322-330. doi:10.2519/jospt.2021.9982
37. Barg, A., Pagenstert, G. I., Hugle, T., Gloyer, M., Wiewiorski, M., Henninger, H. B., & Valderrabano, V. (2013). Ankle osteoarthritis: etiology, diagnostics, and classification. Foot Ankle Clin, 18(3), 411-426. doi:10.1016/j.fcl.2013.06.001
38. Brukner, P., Bradshaw, C., Khan, K. M., White, S., & Crossley, K. (1996). Stress fractures: a review of 180 cases. Clin J Sport Med, 6(2), 85-89. Retrieved from https://pubmed.ncbi.nlm.nih.gov/8673581/
39. Cosman, F., Ruffing, J., Zion, M., Uhorchak, J., Ralston, S., Tendy, S., . . . Nieves, J. (2013). Determinants of stress fracture risk in United States Military Academy cadets. Bone, 55(2), 359-366. doi:10.1016/j.bone.2013.04.011
40. Milgrom, C., Giladi, M., Stein, M., Kashtan, H., Margulies, J. Y., Chisin, R., . . . Aharonson, Z. (1985). Stress fractures in military recruits. A prospective study showing an unusually high incidence. J Bone Joint Surg Br, 67(5), 732-735. doi:10.1302/0301-620X.67B5.4055871
41. Arnold, M. J., & Moody, A. L. (2018). Common Running Injuries: Evaluation and Management. Am Fam Physician, 97(8), 510-516. Retrieved from https://pubmed.ncbi.nlm.nih.gov/29671490/
42. Kahanov, L., Eberman, L. E., Games, K. E., & Wasik, M. (2015). Diagnosis, treatment, and rehabilitation of stress fractures in the lower extremity in runners. Open Access J Sports Med, 6, 87-95. doi:10.2147/OAJSM.S39512.

43. North, K., Potter, M. Q., Kubiak, E. N., Bamberg, S. J., & Hitchcock, R. W. (2012). The effect of partial weight bearing in a walking boot on plantar pressure distribution and center of pressure. Gait Posture, 36(3), 646-649. doi:10.1016/j.gaitpost.2012.04.015
44. Kadel, N. J., Segal, A., Orendurff, M., Shofer, J., & Sangeorzan, B. (2004). The efficacy of two methods of ankle immobilization in reducing gastrocnemius, soleus, and peroneal muscle activity during stance phase of gait. Foot Ankle Int, 25(6), 406-409. doi:10.1177/107110070402500607
45. Bass, J. J., Hardy, E. J. O., Inns, T. B., Wilkinson, D. J., Piasecki, M., Morris, R. H., . . . Phillips, B. E. (2021). Atrophy Resistant vs. Atrophy Susceptible Skeletal Muscles: "aRaS" as a Novel Experimental Paradigm to Study the Mechanisms of Human Disuse Atrophy. Front Physiol, 12, 653060. doi:10.3389/fphys.2021.653060
46. Zellers, J. A., Tucker, L. A., Higginson, J. S., Manal, K., & Gravare Silbernagel, K. (2019). Changes in gait mechanics and muscle activity with wedge height in an orthopaedic boot. Gait Posture, 70, 59-64. doi:10.1016/j.gaitpost.2019.02.027
47. Powell, D., Clowers, K., Keefer, M., Zhang, S. (2012). Alterations in neuromuscular activation patterns associated with walking in short-leg walking boots. Journal of Sport and Health Sciences, 1, 43-48. doi:10.1016/j.jshs.2012.02.003
48. Bailon-Plaza, A., & van der Meulen, M. C. (2003). Beneficial effects of moderate, early loading and adverse effects of delayed or excessive loading on bone healing. J Biomech, 36(8), 1069-1077. doi:10.1016/s0021-9290(03)00117-9
49. Winter, D. A. (1983). Moments of force and mechanical power in jogging. J Biomech, 16(1), 91-97. doi:10.1016/0021-9290(83)90050-7
50. Lopez, R. G., & Jung, H. G. (2015). Achilles tendinosis: treatment options. Clin Orthop Surg, 7(1), 1-7. doi:10.4055/cios.2015.7.1.1
51. Hullfish, T. J., O'Connor, K. M., & Baxter, J. R. (2020). Instrumented immobilizing boot paradigm quantifies reduced Achilles tendon loading during gait. J Biomech, 109, 109925. doi:10.1016/j.jbiomech.2020.109925
52. McCullough, M. B., Ringleb, S. I., Arai, K., Kitaoka, H. B., & Kaufman, K. R. (2011). Moment arms of the ankle throughout the range of motion in three planes. Foot Ankle Int, 32(3), 300-306. doi:10.3113/FAI.2011.0300
53. Honert, E. C., & Zelik, K. E. (2016). Inferring Muscle-Tendon Unit Power from Ankle Joint Power during the Push-Off Phase of Human Walking: Insights from a Multiarticular EMG-Driven Model. PLoS One, 11(10), e0163169. doi:10.1371/journal.pone.0163169
54. Nahm, N., Bey, M. J., Liu, S., & Guthrie, S. T. (2019). Ankle Motion and Offloading in Short Leg Cast and Low and High Fracture Boots. Foot Ankle Int, 40(12), 1416-1423. doi:10.1177/1071100719868721
55. Zhang, S., Clowers, K. G., & Powell, D. (2006). Ground reaction force and 3D biomechanical characteristics of walking in short-leg walkers. Gait Posture, 24(4), 487-492. doi:10.1016/j.gaitpost.2005.12.003
56. Sammarco, J. (1977). Biomechanics of the ankle. I. Surface velocity and instant center of rotation in the sagittal plane. Am J Sports Med, 5(6), 231-234. doi:10.1177/036354657700500603

57. Stauffer, R. N., Chao, E. Y., & Brewster, R. C. (1977). Force and motion analysis of the normal, diseased, and prosthetic ankle joint. Clin Orthop Relat Res(127), 189-196. Retrieved from https://pubmed.ncbi.nlm.nih.gov/912978/
58. Ngoh, K. J., Gouwanda, D., Gopalai, A. A., & Chong, Y. Z. (2018). Estimation of vertical ground reaction force during running using neural network model and uniaxial accelerometer. J Biomech, 76, 269-273. doi:10.1016/j.jbiomech.2018.06.006
59. Shahabpoor, E., Pavic, A., Brownjohn, J. M. W., Billings, S. A., Guo, L. Z., & Bocian, M. (2018). Real-Life Measurement of Tri-Axial Walking Ground Reaction Forces Using Optimal Network of Wearable Inertial Measurement Units. IEEE Trans Neural Syst Rehabil Eng, 26(6), 1243-1253. doi:10.1109/TNSRE.2018.2830976
60. Burr, D. B., Milgrom, C., Fyhrie, D., Forwood, M., Nyska, M., Finestone, A., . . . Simkin, A. (1996). In vivo measurement of human tibial strains during vigorous activity. Bone, 18(5), 405-410. doi:10.1016/8756-3282(96)00028-2
61. Lanyon, L. E., Hampson, W. G., Goodship, A. E., & Shah, J. S. (1975). Bone deformation recorded in vivo from strain gauges attached to the human tibial shaft. Acta Orthop Scand, 46(2), 256-268. doi:10.3109/17453677508989216
62. Milgrom, C., Finestone, A., Simkin, A., Ekenman, I., Mendelson, S., Millgram, M., . . . Burr, D. (2000). In-vivo strain measurements to evaluate the strengthening potential of exercises on the tibial bone. J Bone Joint Surg Br, 82(4), 591-594. doi:10.1302/0301-620x.82b4.9677
63. Milgrom, C., Burr, D. B., Finestone, A. S., & Voloshin, A. (2015). Understanding the etiology of the posteromedial tibial stress fracture. Bone, 78, 11-14. doi:10.1016/j.bone.2015.04.033
64. Meardon, S. A., Edwards, B., Ward, E., & Derrick, T. R. (2009). Effects of custom and semi-custom foot orthotics on second metatarsal bone strain during dynamic gait simulation. Foot Ankle Int, 30(10), 998-1004. doi:10.3113/FAI.2009.0998
65. Batt, M. E., Kemp, S., & Kerslake, R. (2001). Delayed union stress fractures of the anterior tibia: conservative management. Br J Sports Med, 35(1), 74-77. doi:10.1136/bjsm.35.1.74
66. Plasschaert, V. F., Johansson, C. G., & Micheli, L. J. (1995). Anterior tibial stress fracture treated with intramedullary nailing: a case report. Clin J Sport Med, 5(1), 58-61; discussion 61-52. doi:10.1097/00042752-199501000-00011
67. Saunier, J., & Chapurlat, R. (2018). Stress fracture in athletes. Joint Bone Spine, 85(3), 307-310. doi:10.1016/j.jbspin.2017.04.013
68. Arendt, E., Agel, J., Heikes, C., & Griffiths, H. (2003). Stress injuries to bone in college athletes: a retrospective review of experience at a single institution. Am J Sports Med, 31(6), 959-968. doi:10.1177/03635465030310063601
69. Burr, D. B., Milgrom, C., Fyhrie, D., Forwood, M., Nyska, M., Finestone, A., . . . Simkin, A. (1996). In vivo measurement of human tibial strains during vigorous activity. Bone, 18(5), 405-410. doi:10.1016/8756-3282(96)00028-2
70. Ekenman, I., Milgrom, C., Finestone, A., Begin, M., Olin, C., Arndt, T., & Burr, D. (2002). The role of biomechanical shoe orthoses in tibial stress fracture prevention. Am J Sports Med, 30(6), 866-870.

doi:10.1177/03635465020300061801
71. Milgrom, C., Finestone, A., Sharkey, N., Hamel, A., Mandes, V., Burr, D., . . . Ekenman, I. (2002). Metatarsal strains are sufficient to cause fatigue fracture during cyclic overloading. Foot Ankle Int, 23(3), 230-235. doi:10.1177/107110070202300307
72. Hadid, A., Epstein, Y., Shabshin, N., & Gefen, A. (2018). Biomechanical Model for Stress Fracture-related Factors in Athletes and Soldiers. Med Sci Sports Exerc, 50(9), 1827-1836. doi:10.1249/MSS.0000000000001628
73. Milgrom, C., Radeva-Petrova, D. R., Finestone, A., Nyska, M., Mendelson, S., Benjuya, N., . . . Burr, D. (2007). The effect of muscle fatigue on in vivo tibial strains. J Biomech, 40(4), 845-850. doi:10.1016/j.jbiomech.2006.03.006
74. Turner, C. H., Wang, T., & Burr, D. B. (2001). Shear strength and fatigue properties of human cortical bone determined from pure shear tests. Calcif Tissue Int, 69(6), 373-378. doi:10.1007/s00223-001-1006-1.
75. Bennett J. E., Reinking M. F., Pluemer B., Pentel A., Seaton M., Killian C. (2001). Factors contributing to the development of medial tibial stress syndrome in high school runners. J Ortho Sports Phys Ther. 31(9):504-10. https://www.jospt.org/doi/abs/10.2519/jospt.2001.31.9.504
76. Qualisys AB. (2011) Qualisys Track Manager User Manual. Retrieved from https://www.qualisys.com/cameras/5-6-7/ on July 21, 2021.
77. Novel Electronics. (2021) loadsol®: plantar normal force inside footwear. Retrieved from https://www.novel.de/products/loadsol/ on July 21, 2021.
78. JR3 Multi-Axis Load Cell Technologies. (2021). https://www.jr3.com/resources/specification-sheets.
79. Micro-Measurements. (2021) Linear strain gauge 235SL. Retrieved from https://micro-measurements.com/pca/detail/235sl on July 21, in November 2021.
80. National Instruments. (2021) NI-9235 C Series Strain Quarter Bridge Module. Retrieved from https://www.ni.com/docs/en-US/bundle/ni-9235-specs/page/specs.html in November 2021.
81. National Instruments. (2021) cDAQ 9171 CompactDAQ Chassis. Retrieved from https://www.ni.com/docs/en-US/bundle/cdaq-9171-specs/page/specs.html in November 2021.

APPENDIX A. SPECIFICATIONS

This appendix provides specifications of the equipment (**Table A-1**) used throughout this body of work.

Table A-1. Equipment Specifications.

System Information	Specifications
Qualysis cameras Oqus 3	Sampling frequency: 240 Hz Full resolution of 1280x1024 Normal mode (full FOV): 1.3 MP, 500 fps High-speed mode (full FOV): 0.3 MP, 1750 fps Max capture distance: 22 mm
Loadsol insoles Various sizes	Sampling frequency: 100Hz Force-range: 0 – 2550 N Resolution: 10N Calibrated accuracy: ±5%
Load Cell JR3 Multi-Axis Force-Torque Sensor Model: 67M25S3 Mechanical Load Rating: 130 lb	X-Axis and Y-Axis Force Readings Standard Measurement Range: ±130 lb Digital Resolution: 0.033 lb Single-Axis Overload: 550 lb Z-Axis Force Readings Standard Measurement Range: ±260 lb Digital Resolution: 0.065 lb Single-Axis Overload: 2300 lb
Strain Gauges Micro-Measurements Item Code: MMF404429	Series: C4A Resistance: 120 Ω Gage Factor: 2.04 STC: 13,06,13,00
NI 9235	Number of Channels: 8 analog inputs Quarter Bridge 120 Ω ADC resolution: 24 bits Data rate range: 794 – 10k samples/sec
NI cDAQ 9171 C-series module	Maximum sample rate: Determined by the C Series module Timing accuracy: 50ppm of sample rate Timing resolution: 12.5 ns

Table A-1. Continued.

Source data:

Qualisys AB. (2011) Qualisys Track Manager User Manual. Retrieved from https://www.qualisys.com/hardware/5-6-7/ on July 21, 2021 [76].

Novel Electronics. (2021) loadsol®: plantar normal force inside footwear. Retrieved from https://www.novel.de/products/loadsol/ on July 21, 2021 [77].

Sources: JR3 Multi-Axis Load Cell Technologies. (2021). https://www.jr3.com/resources/specification-sheets [78].

Micro-Measurements. (2021) Linear strain gauge 235SL. Retrieved from https://micro-measurements.com/pca/detail/235sl on July 21, in November 2021 [79].

National Instruments. (2021) NI-9235 C Series Strain Quarter Bridge Module. Retrieved from https://www.ni.com/docs/en-US/bundle/ni-9235-specs/page/specs.html in November 2021 [80.

National Instruments. (2021) cDAQ 9171 CompactDAQ Chassis. Retrieved from https://www.ni.com/docs/en-US/bundle/cdaq-9171-specs/page/specs.html in November 2021 [81].

APPENDIX B. EXTENDED METHODOLOGY OF STUDY 1 AND STUDY 2

This appendix provides additional information regarding the equipment used during the treadmill walking study described in Chapter 3 and the cadaveric study described in Chapter 4. Due to brace design, retro-reflective markers were positioned on the posterior aspect of the DAO (**Figure B-1**) and on the posterior-lateral aspect of the shank when wearing the walking boot (**Figure B-2**) for multiple motion capture cameras to detect the motion of the shank during treadmill walking. The walking boot was adapted to expose the heel and retro-reflective markers positioned directly on the skin. The purpose of this was to track the motion of the foot during treadmill walking rather than the motion of the boot. Doing so provided information that the patient is able to articulate their foot slightly while wearing the walking boot. **Figure B-3** shows the treadmill walking activity. **Figure B-4** shows sample motion capture data. **Figure B-5** is the Brace comfort score survey that each participant filled out to quantify the comfort level of each brace condition. **Figure B-6** shows the testing set up with the cadaver specimen wearing the DAO and walking boot. **Figure B-7** shows the Achilles tendon dead weight during testing set up.

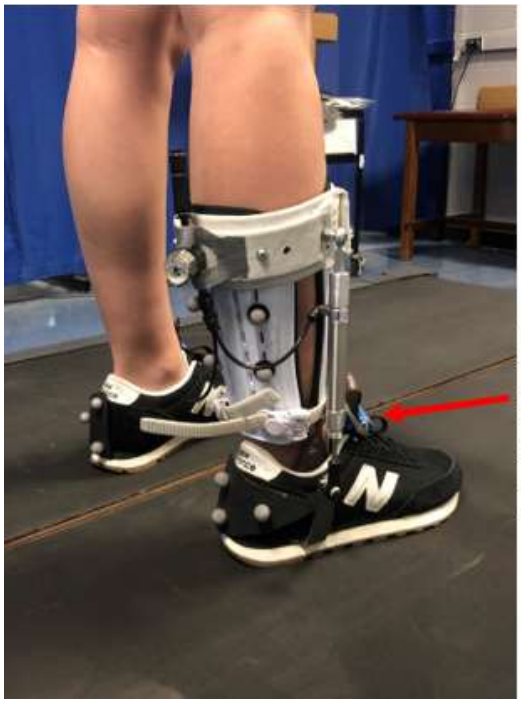

Figure B-1. Equipment and Setup in DAO for Study 1.
DAO: Dynamic Ankle Orthosis.

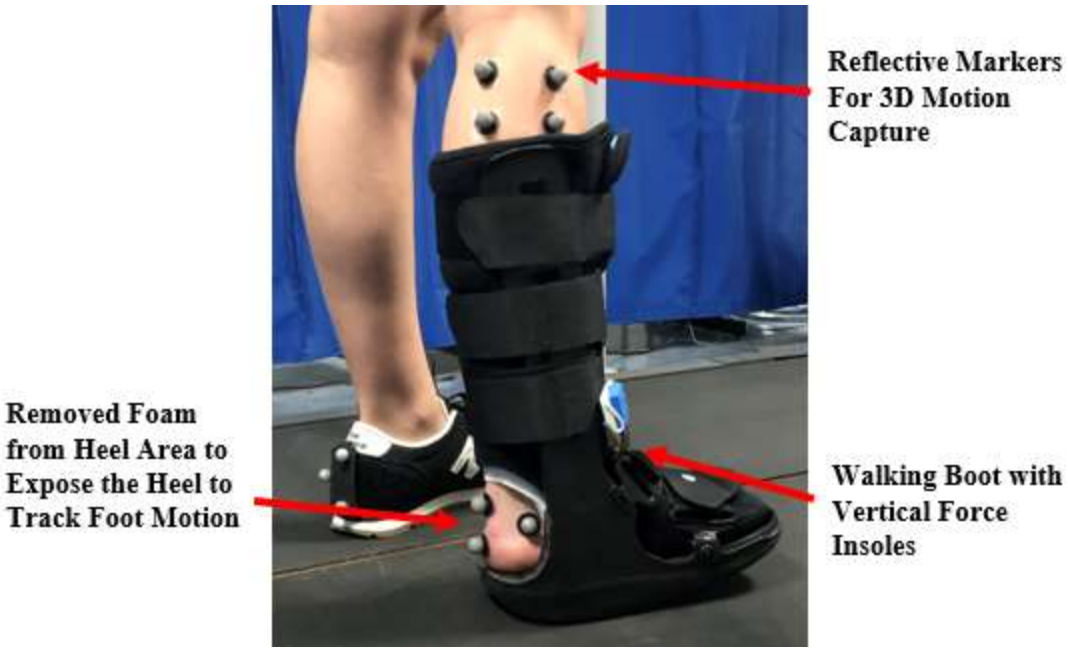

Figure B-2. Equipment and Setup in Walking Boot for Study 1.
Indication of segment tracking markers and Loadsol insole.

Figure B-3. Treadmill Walking During Data Collection for Study 1.

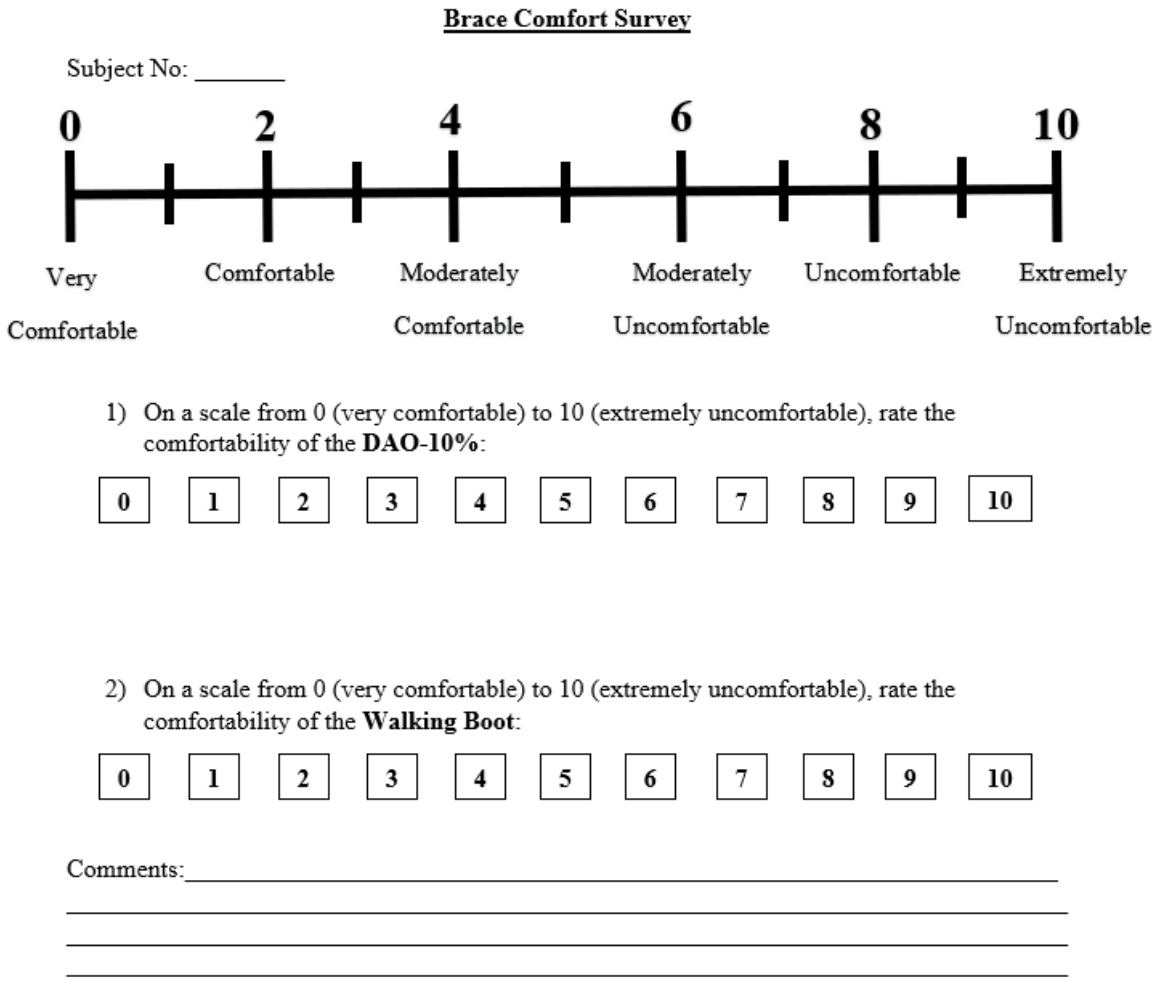

Figure B-4. Brace Comfort Score Survey Used to Quantify the Comfort Level of Each Brace Condition.
Participants scored the comfort of each brace condition at the end of each walking task.

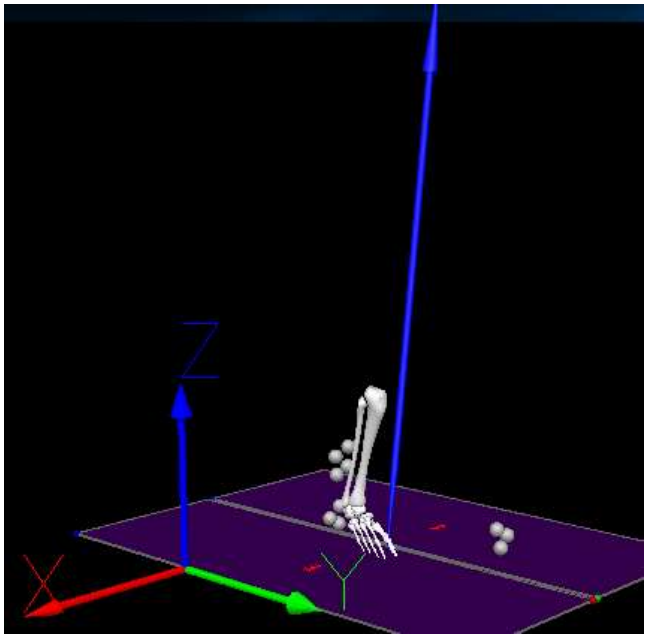

Figure B-5. Sample Visual 3D Model Reconstruction of Motion Capture Data During Treadmill Walking.

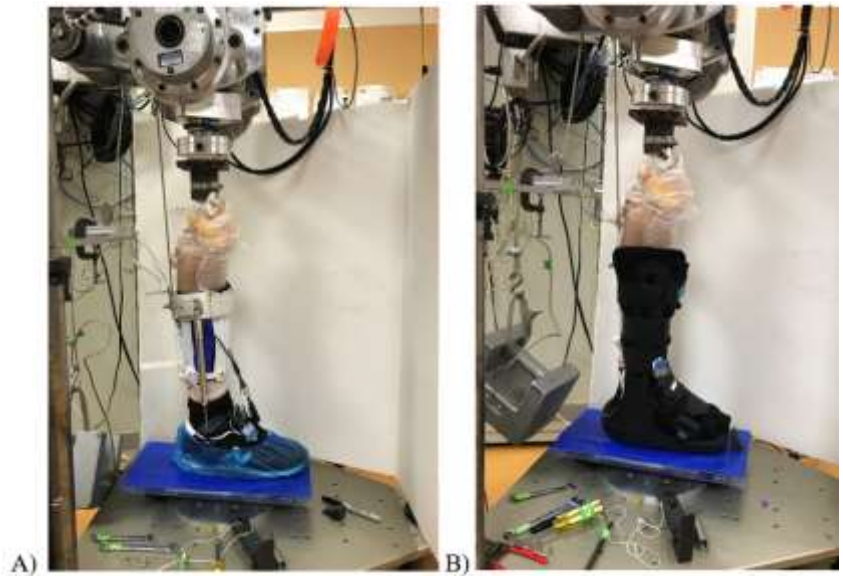

Figure B-6. Cadaver Specimen (S1) Positioned in Robotic Testing Platform Wearing Bracing Conditions for Study 2.
DAO: Dynamic Ankle Orthosis. A) DAO and B) Walking Boot.

Figure B-7. Posterior View of Testing Setup Showing the Static Achilles Load for Study 2.

During preliminary testing, strain rate and insole loading rate were two parameters that we sought to collect. The loading rate was investigated to replicate a similar physiological loading rate that was observed in the treadmill walking study (**Chapter 3**). Moving the robot under a "load control" command, the actuator will apply a uniaxial load until the load cell sensor detects a specified load limit. Moving the robot under a "MOVES command," the actuator will move between two specified positions in space. When running the robot at its maximum capacity (500%), we were unable to replicate a similar insole loading rate that was observed during the treadmill walking study (**Figure B-8**). Additionally, strain rate was a desirable parameter to determine if there was any correlation between the strain rate and vertical accelerations using an IMeasureU Blue Trident inertial measurement unit (IMU; Vicon Motion Systems Ltd, Oxford, UK). Because the vertical travel distance of the robot actuator was limited, the robot was not able to produce a strong enough dynamic impact when loading the cadaveric tissue to elicit a response from the IMU. **Figures B-9** and **B-10** show sample strain data of the cadaver specimen when wearing the DAO and Walking boot.

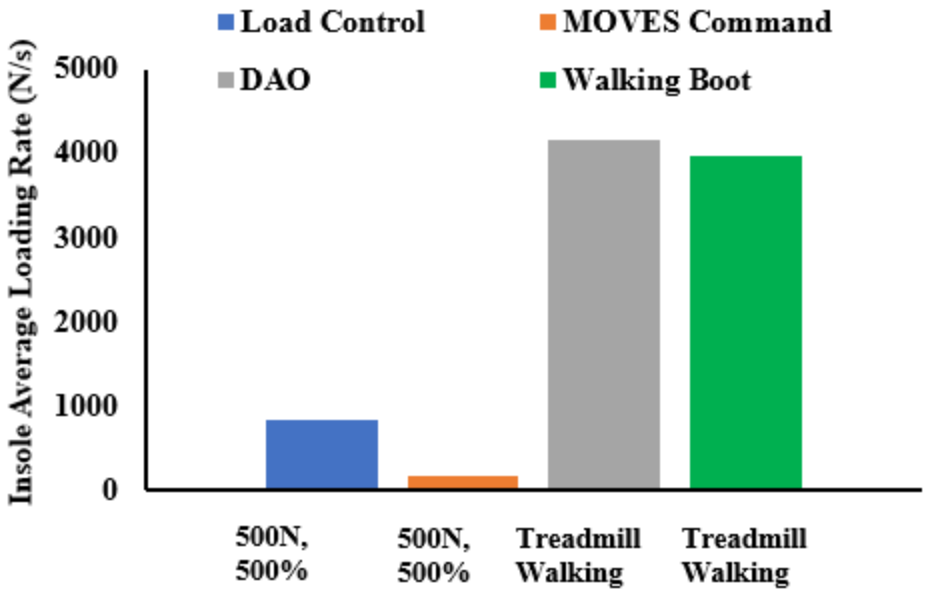

Figure B-8. Comparison of Vertical Force Insole Loading Rate Between the Robotic Testing Platform and Treadmill Walking.
Testing the cadaveric specimens in the robotic testing platform (Blue and Orange) for study 2 (with no brace intervention) compared to the participant vertical force insole loading rate when wearing the DAO (Grey) and Walking Boot (Green) during treadmill walking.

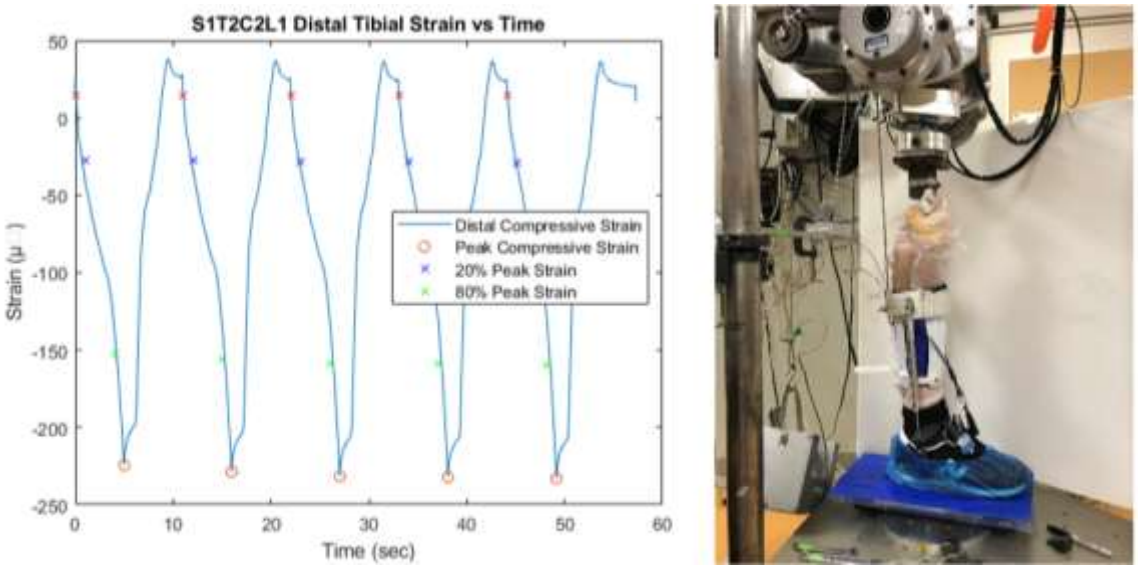

Figure B-9. Sample Strain Magnitude for the DAO During Uniaxial Dynamic Loading at the Distal Tibia for Study 2.
DAO: Dynamic Ankle Orthosis.

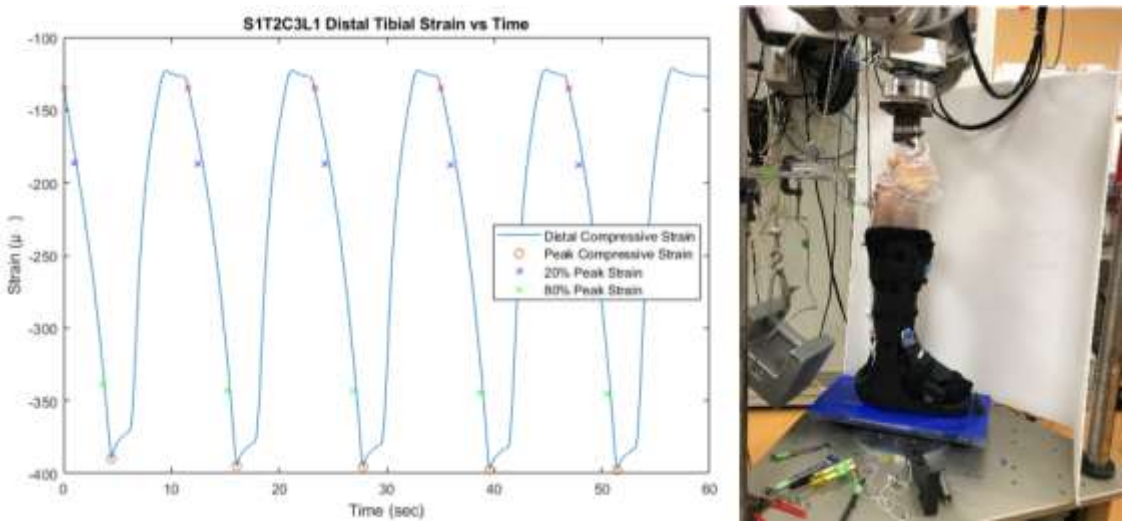

Figure B-10. Sample Strain Magnitude for the Walking Boot During Uniaxial Dynamic Loading at the Distal Tibia for Study 2.

APPENDIX C. EXTENDED RESULTS OF STUDY 1 AND STUDY 2

For the purposes of this study the primary objective was to determine the peak tibial compressive force at peak plantarflexor moment. Each parameter that was used to calculate the tibial compressive force is provided in **Table C-1** showing the difference in the moment arms between brace conditions. The entire stance phase was captured during treadmill walking. **Figure C-1** shows that there was a significant moderate reduction in the peak VRF ($p = 0.002$, $d = 0.73$) during the first half of stance phase when wearing the DAO compared to the walking boot. The rigid design of the walking boot transfers more force to the lower limb and TSF during load acceptance. **Figure C-2** shows how wearing the DAO affected the tibial compressive force in each individual participant compared to wearing the walking boot. Over half of the participants showed reductions in the tibial compressive force when wearing the DAO. Three participants had an increase in the tibial compressive force when wearing the DAO compared to the walking boot.

During preliminary testing, the strain magnitude was significantly reduced at the distal tibia in during static conditions (**Figure C-3**) in the DAO ($p = 0.013$, $d = 3.48$) compared to the walking boot. **Figure C-4 s**hows that the DAO was able to significantly reduce the strain rate at the distal tibia ($p = 0.035$, $d = 2.06$) and midshaft tibia ($p = 0.031$, $d = 2.21$) in the DAO compared to the walking boot.

Table C-1. Kinetics and Kinematics in the DAO and Walking Boot During Treadmill Walking.

Variables	DAO	Walking Boot
Linear Acceleration Moment Arm (m)	0.042 ± 0.006	0.051 ± 0.009
Vertical Acceleration Moment Arm (m)	0.053 ± 0.003	0.065 ± 0.013
Peak Propulsive Force (N)	81.2 ± 17.4	69.8 ± 15.0
Propulsive Force Moment Arm (m)	0.13 ± 0.01	0.16 ± 0.01
VRF_z (N)	598.2 ± 110.8	596.8 ± 127.2
VRF_z Moment Arm (m)	0.18 ± 0.01	0.20 ± 0.02
Achilles Tendon Moment Arm (m)	0.03 ± 0.01	0.03 ± 0.01
Summation of Horizontal Force at Ankle (N)	-68.3 ± 15.0	-64.087 ± 14.3
Summation of Vertical Force at Ankle (N)	-583.6 ± 109.7	-585.5 ± 125.6
Tibial angle at Peak Plantar Flexion Moment (deg)	26.6 ± 1.7	30.2 ± 4.0
Force along Tibial Axis (N)	652.4 ± 119.4	679.1 ± 143.1
Ankle Moment (N*m)	-118.7 ± 22.6	-133.8 ± 33.2
Achilles Tendon Force (N)	3955.4 ± 877.7	4493.7 ± 1365.2
Peak Tibial Compressive Force (N)	4607.8 ± 947.7	5172.8 ± 1466.2

Mean ± Standard Deviation. DAO: Dynamic Ankle Orthosis. VRF: Vertical Reaction Force.

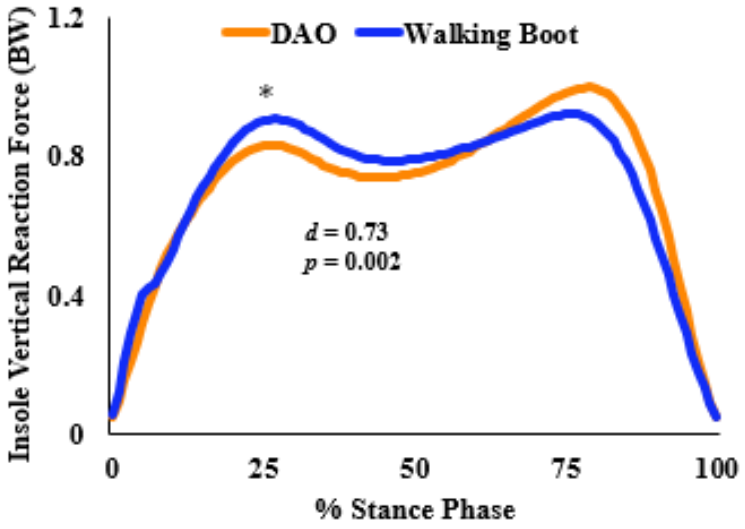

Figure C-1. Insole Vertical Reaction Force (BW) During Stance Time Between the DAO and Walking Boot. Showing a Significant Reduction in the Peak Vertical Reaction Force in the First Fifty Percent of Stance Phase.
DAO: Dynamic Ankle Orthosis.

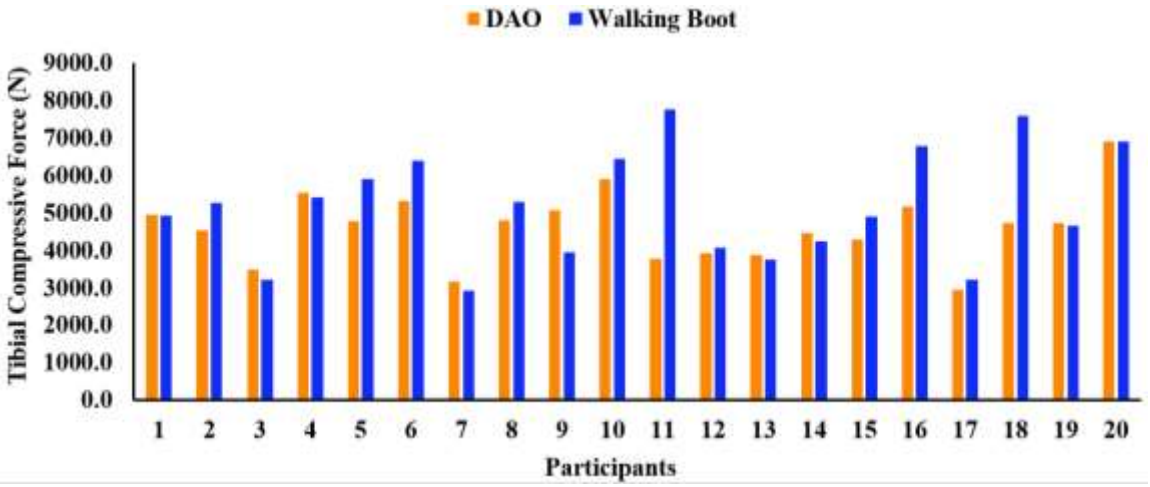

Figure C-2. Tibial Compressive Force (N) When Wearing the DAO and Walking Boot for Each Participant.
DAO: Dynamic Ankle Orthosis.

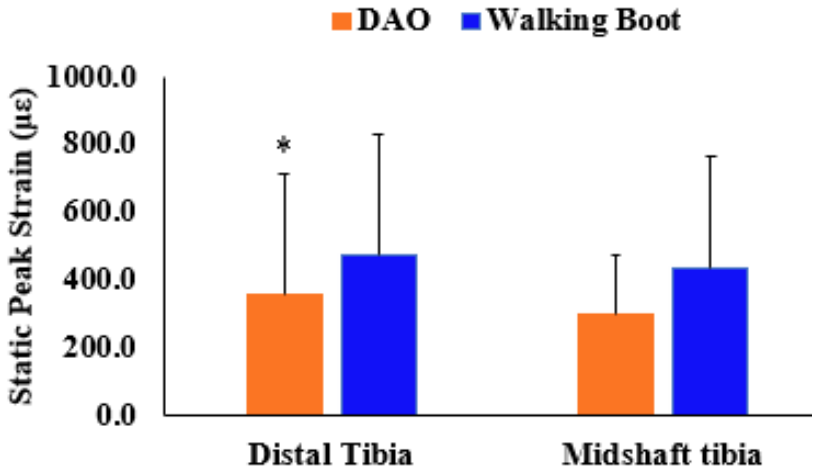

Figure C-3. Peak Strain (με) During Static Uniaxial Loading Between Brace Conditions: DAO and Walking Boot; and Strain Gauge Locations: Distal and Midshaft Tibia.
DAO: Dynamic Ankle Orthosis.

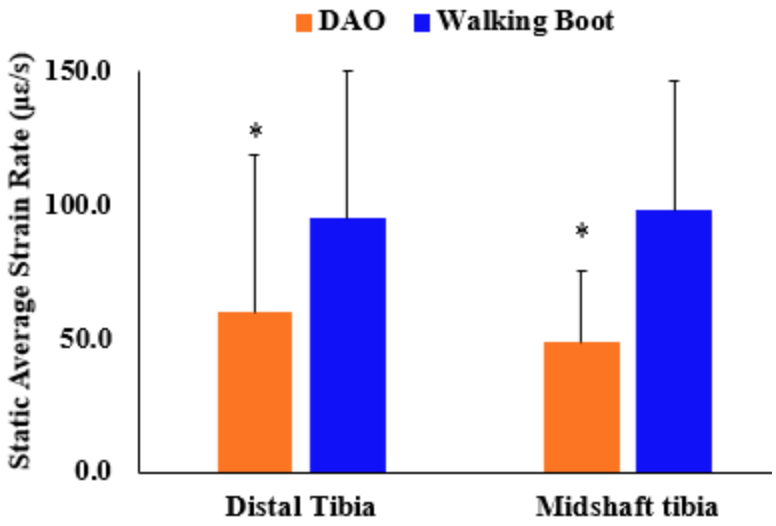

Figure C-4 Average Strain Rate (με/s) During Static Uniaxial Loading Between Brace Conditions: DAO and Walking Boot; and Strain Gauge Locations: Distal Tibia and Midshaft Tibia.
DAO: Dynamic Ankle Orthosis

VITA

Perri was born in St. Louis, MO in 1996. He was raised in Florissant, MO where he graduated from Saint Louis University High in 2015. He attended University of Indianapolis – Indiana University Purdue University Indianapolis and graduated cum laude with a Dual Bachelor of Science degree in Mechanical Engineering and Mathematics in 2020. He then attended graduate school at the University of Tennessee Health Science Center (UTHSC) where he was the recipient of the "Lee and Jennie Boaumont Scholarship" award.

Perri performed graduate research under the tutelage of his advisor, Dr. Denis DiAngelo in the Orthopedic BioRobotics and Rehabilitation laboratory, a well-established lab with a history of advanced biomechanical evaluation of surgical implants. Perri's research extended beyond the scope of surgical implants to include the study of non-surgical medical orthosis. During the scope of his graduate work, Perri collaborated with fellow scientists, and practitioners to evaluate new orthopedic technology. Following approval of this thesis, Perri expects to receive his Master of Science in Biomedical Engineering in December 2022.

Driven by the desire to continue his education and study of biomedical devices, biomechanical analysis, and movement science, Perri chose to pursue his doctor and continue his research in the UTHSC Orthopedic BioRobotics and Rehabilitation Laboratory. Perri will collaborate with fellow scientists, clinicians, and practitioners to study the effects of and develop new orthopedic technology for tibial stress fractures and degenerative joint diseases of the lower limb, foot, and ankle.